ARL

US Army Research Laboratory

High-Rate Mechanical Properties of JA2 Propellant at Temperatures from –50 to 80 °C

by Stephen L Howard, Michael G Leadore, and Joyce E Newberry

NOTICES

Disclaimers

The findings in this report are not to be construed as an official Department of the Army position unless so designated by other authorized documents.

Citation of manufacturer's or trade names does not constitute an official endorsement or approval of the use thereof.

Destroy this report when it is no longer needed. Do not return it to the originator.

ARL

High-Rate Mechanical Properties of JA2 Propellant at Temperatures from –50 to 80 °C

by Stephen L Howard, Michael G Leadore, and
Joyce E Newberry
Weapons and Materials Research Directorate, ARL

REPORT DOCUMENTATION PAGE		*Form Approved* *OMB No. 0704-0188*

Public reporting burden for this collection of information is estimated to average 1 hour per response, including the time for reviewing instructions, searching existing data sources, gathering and maintaining the data needed, and completing and reviewing the collection information. Send comments regarding this burden estimate or any other aspect of this collection of information, including suggestions for reducing the burden, to Department of Defense, Washington Headquarters Services, Directorate for Information Operations and Reports (0704-0188), 1215 Jefferson Davis Highway, Suite 1204, Arlington, VA 22202-4302. Respondents should be aware that notwithstanding any other provision of law, no person shall be subject to any penalty for failing to comply with a collection of information if it does not display a currently valid OMB control number.
PLEASE DO NOT RETURN YOUR FORM TO THE ABOVE ADDRESS.

1. REPORT DATE *(DD-MM-YYYY)*	2. REPORT TYPE	3. DATES COVERED (From - To)
July 2015	Memorandum	January 2011–January 2015

4. TITLE AND SUBTITLE	5a. CONTRACT NUMBER
High-Rate Mechanical Properties of JA2 Propellant at Temperatures from –50 to 80 °C	
	5b. GRANT NUMBER
	5c. PROGRAM ELEMENT NUMBER

6. AUTHOR(S)	5d. PROJECT NUMBER
Stephen L Howard, Michael G Leadore, and Joyce E Newberry	622618.H8000
	5e. TASK NUMBER
	5f. WORK UNIT NUMBER

7. PERFORMING ORGANIZATION NAME(S) AND ADDRESS(ES)	8. PERFORMING ORGANIZATION REPORT NUMBER
US Army Research Laboratory ATTN: RDRL-WML-D Aberdeen Proving Ground, MD 21005-5069	ARL-MR-0894

9. SPONSORING/MONITORING AGENCY NAME(S) AND ADDRESS(ES)	10. SPONSOR/MONITOR'S ACRONYM(S)
	11. SPONSOR/MONITOR'S REPORT NUMBER(S)

12. DISTRIBUTION/AVAILABILITY STATEMENT
Approved for public release; distribution is unlimited.

13. SUPPLEMENTARY NOTES

14. ABSTRACT

JA2, a viscoelastic polymeric propellant, was studied with uniaxial compression to approximately 70% engineering strain at a strain rate of approximately 100 s^{-1} at each decade of temperature from –50 to 80 °C. Each sample after postcompression relaxation was cold-cleaved for postmortem examination. The stress/strain curves and postmortem examination showed the trend of reduced ductility as the temperature decreased. The stress/strain curves of all temperatures showed that a strain of approximately 35% would allow the sample to deform without achieving the point of failure. Compression experiments at selected temperatures were repeated with a limit of this strain. Postmortem examination of the cold-cleaved grains was performed using scanning electron microscopy, the results of which showed the transitions from viscous flow to void and tear formation to crack tip propagation prior to structural failure of the sample.

15. SUBJECT TERMS

high strain-rate uniaxial compression, mechanical properties, JA2 propellant, viscoelastic polymer, constitutive properties

16. SECURITY CLASSIFICATION OF:			17. LIMITATION OF ABSTRACT	18. NUMBER OF PAGES	19a. NAME OF RESPONSIBLE PERSON
a. REPORT	b. ABSTRACT	c. THIS PAGE	UU	52	Stephen L Howard
					19b. TELEPHONE NUMBER (Include area code)
Unclassified	Unclassified	Unclassified			410-278-6098

Standard Form 298 (Rev. 8/98)
Prescribed by ANSI Std. Z39.18

Contents

List of Figures

List of Tables

1. Introduction

Because propellant mechanical properties are not static but rather functions of temperature (also functions of strain, strain rate, temperature gradient, time, etc.), determination of the mechanical properties of propellants is needed to determine processing/fabrication parameters, physical shape degradation in storage, physical failure during the ballistic cycle, and/or demilitarization/material recycling. A majority of the mechanical property needs can therefore be linked to safe operation during each element of the life cycle of the propellant. JA2, a relatively simple viscoelastic gun propellant, has received attention because of its simplified structure and has been used as a reference baseline for evaluation of other propellants.[1–6] In addition, temperature extremes for both storage and service use of weapon systems have expanded in recent years. Therefore, the temperature range at cogent strain rates also needs to be expanded, especially for baseline references.

This report provides the primary data for mechanical property determination of virgin large-caliber 7-perforation JA2 grains as a function of temperature from –50 to 80 °C at a ballistically relevant strain rate of approximately 100 s^{-1} (this strain rate is considered to be representative of the conditions present in a typical large-caliber gun interior ballistic cycle).[7] This temperature range includes most of the temperatures encountered by typical munitions in either service or storage conditions. Engineering stress/strain curves at each decade of temperature in this range are expected to traverse the glass-transition temperature regime and access properties nearing the viscous flow regime. These properties, properly coupled with interior ballistic calculations, can be used to predict safe gun firing conditions. These mechanical property data will be added to the US Army Research Laboratory database of similar mechanical property data at this strain rate for many propellants.

It is understood that during a ballistic event, propellant grains in a munition typically experience bed movement and collisions with gun wall components as well as with other grains during the ballistic cycle. These impacts are dynamic events that place all or part of each impacted grain in compression. Therefore, the mechanical properties were obtained via high-rate uniaxial compression to simulate these impact events.

2.   Experimental

The Material Test Systems Servo-Hydraulic Tester (MTS-SHT) shown schematically in Fig. 1 was used to obtain the high-rate uniaxial compressive mechanical response[6–9] of the virgin JA2 propellant samples, lot no. RAD-PE-792-71. The JA2 granular propellant (see Fig. 2) was manufactured as right-circular cylinders with 7 perforations. The average grain diameter was 7.5 mm and the length was 16 mm. The perforation diameter was measured at 0.69 mm.
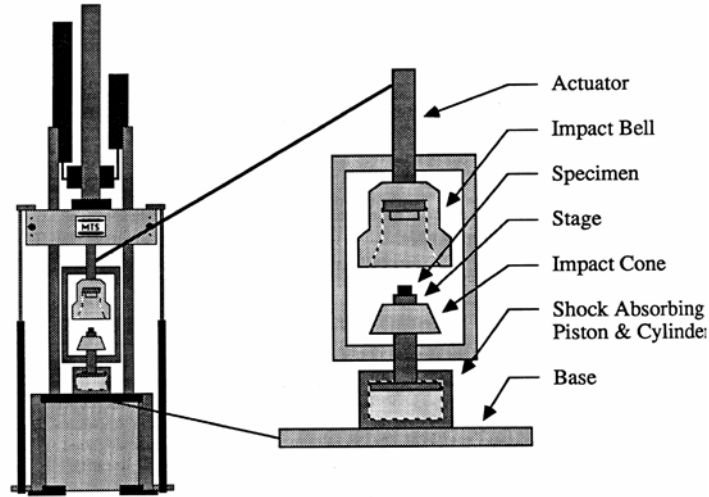
Fig. 1   High-rate MTS-SHT apparatus
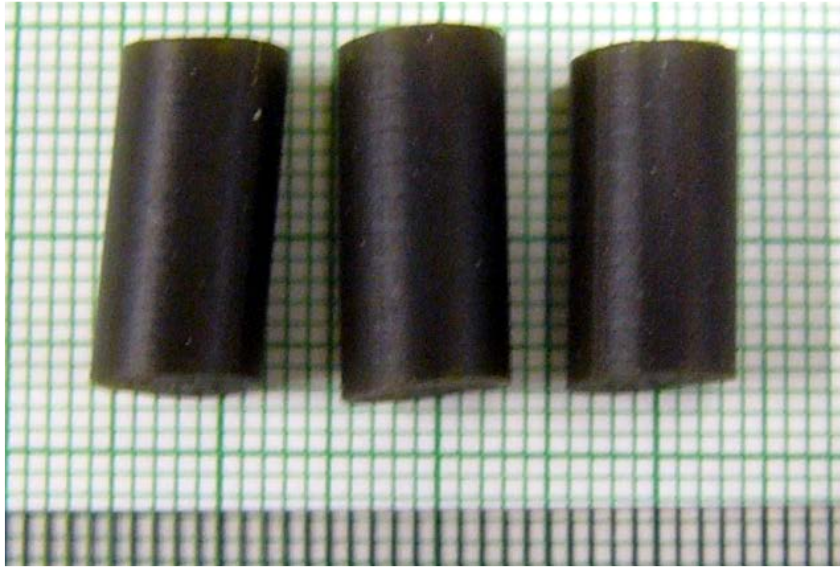
Fig. 2   Propellant grains as received, scale in millimeters

The propellant grains were first prepared into test specimens with an Isomet low-speed diamond-blade saw.[10] To ensure that specimen ends were machined to be flat, mutually parallel, and perpendicular to the extruded axis, 2 new diamond blades were placed on the spindle of the saw spaced 9 mm apart. The specimen grain was then placed in the grain holder and allowed to pass between the 2 blades during saw operation so that both ends were simultaneously cut. The finished test specimens had a length-to-diameter ratio of approximately 1.2 (Fig. 3).
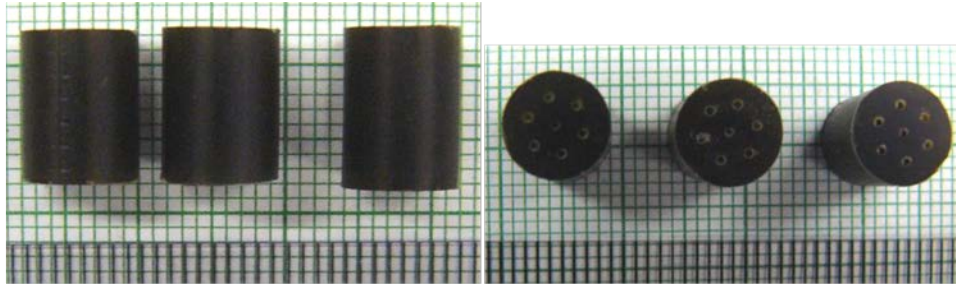
Fig. 3   Finished specimen propellant grains, scale in millimeters

Single-grain specimens for uniaxial compressive tests (Fig. 4) were placed on the specimen stage for each test. A previous study with JA2 indicated that lubrication of the platens had little effect on the mechanical properties.[4] The Joint Army Navy NASA Air Force standard[11] requires that lubrication not be used for propellant samples. Therefore, lubrication of the sample end faces was not performed. The compressive tests were conducted at atmospheric pressure. An average strain rate of approximately 100 s^{-1} was used to compress the specimens to failure (generally about 50% or greater strain for most of the samples). After the compression experiment, the sample was recovered (Fig. 5) for comparison and postmortem analysis.

Fig. 4   Specimen loaded on stage of MTS-SHT apparatus

| –10 °C | –40 °C |

Fig. 5   Postexperiment specimen on stage of MTS-SHT apparatus prior to fragment recovery

The environmental chamber used to temperature-condition the JA2 propellant test specimens was a Thermotron-series model SE-300 chamber with a model 8800 programmer controller that regulated the temperature from –50 to 80 °C. The test specimens were placed into the chamber while at ambient temperature, and the temperature chamber then was regulated to the desired test temperature. Thermocouples were used to measure both air temperature and specimen temperature. The temperature was ramped at a rate of approximately 1 °C/min. When the specified temperature was achieved for both air and specimen, the specimens were conditioned for 1 h before the high-rate testing commenced.

The electron microscope used for this study was an International Scientific Instruments, Inc., SS40 scanning electron microscope (SEM). The electron energy was 10 kV. The samples were cold-cathode sputtered with a gold/palladium alloy prior to examination. The metallic coating was a few atoms thick but allowed electrical conduction to ground of excess electrons, which would otherwise affect image quality. Image magnification was typically 10× to 50× for this report.

3.   Results and Discussion

MTS-SHT mechanical property experiments were conducted on a minimum of 3 specimens at each temperature. An approximate strain rate of 100 s^{-1} was achieved. The specimens were temperature conditioned and uniaxially compressed to failure at ambient pressure to a maximum of 70% end strain. The resulting engineering stress/engineering strain plots are shown in Figs. 6–19. Photographs of the retained specimens after compression also were recorded (Figs. 21–34).
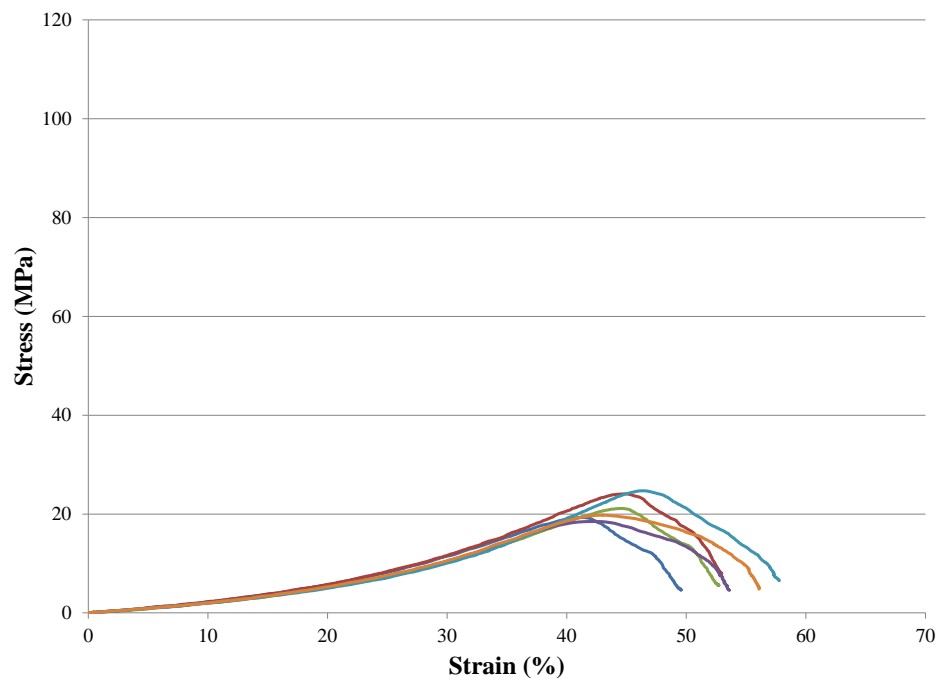
Fig. 6   Typical stress-strain curves for JA2 at a rate of ~100 s^{-1} obtained at 80 °C
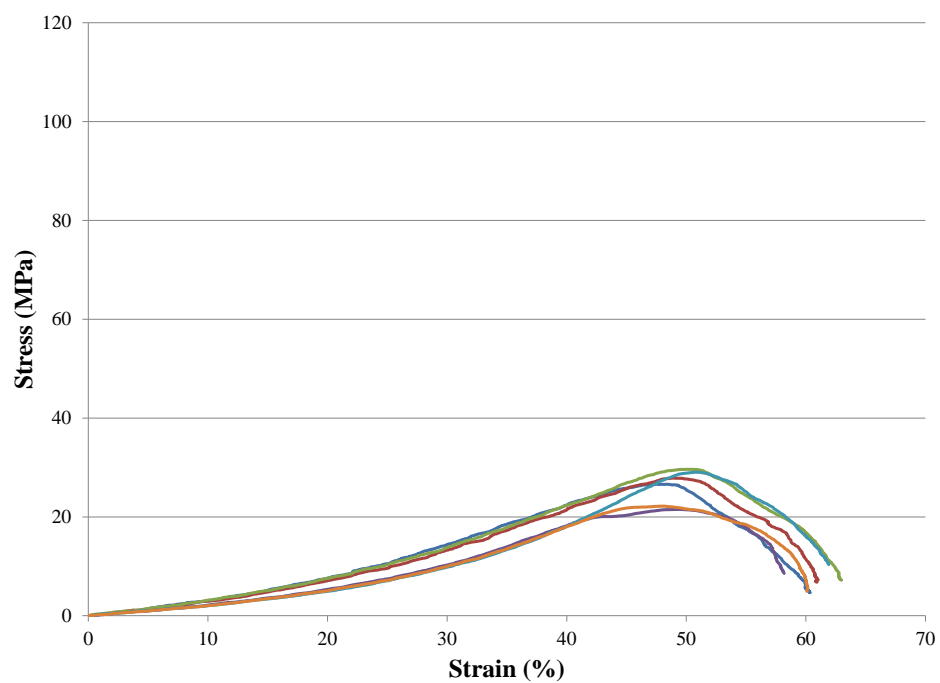
Fig. 7   Typical stress-strain curves for JA2 at a rate of ~100 s^{-1} obtained at 70 °C
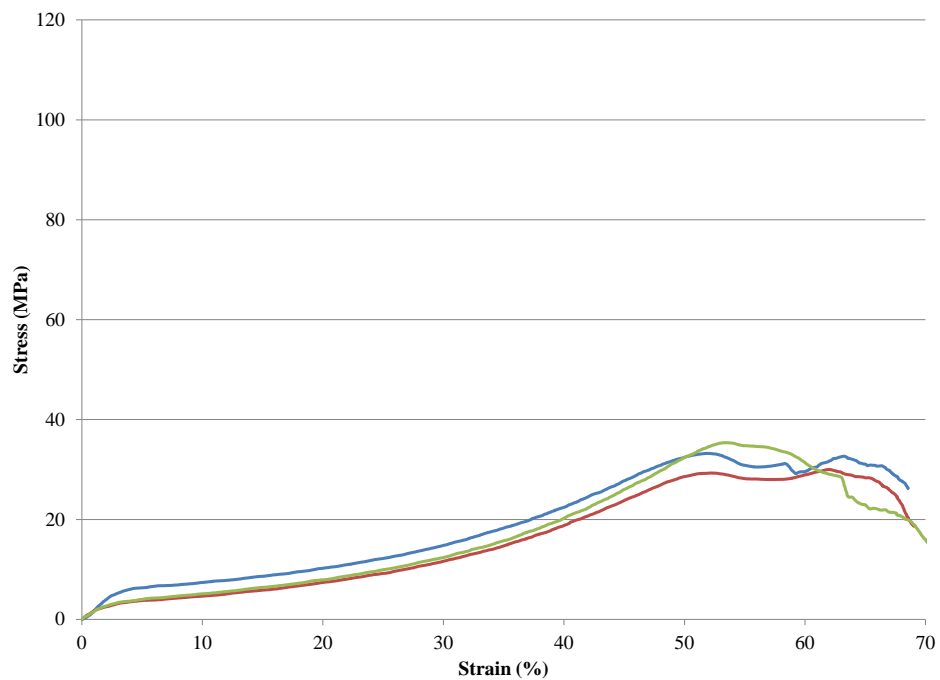
Fig. 8   Typical stress-strain curves for JA2 at a rate of ~100 s⁻¹ obtained at 60 °C
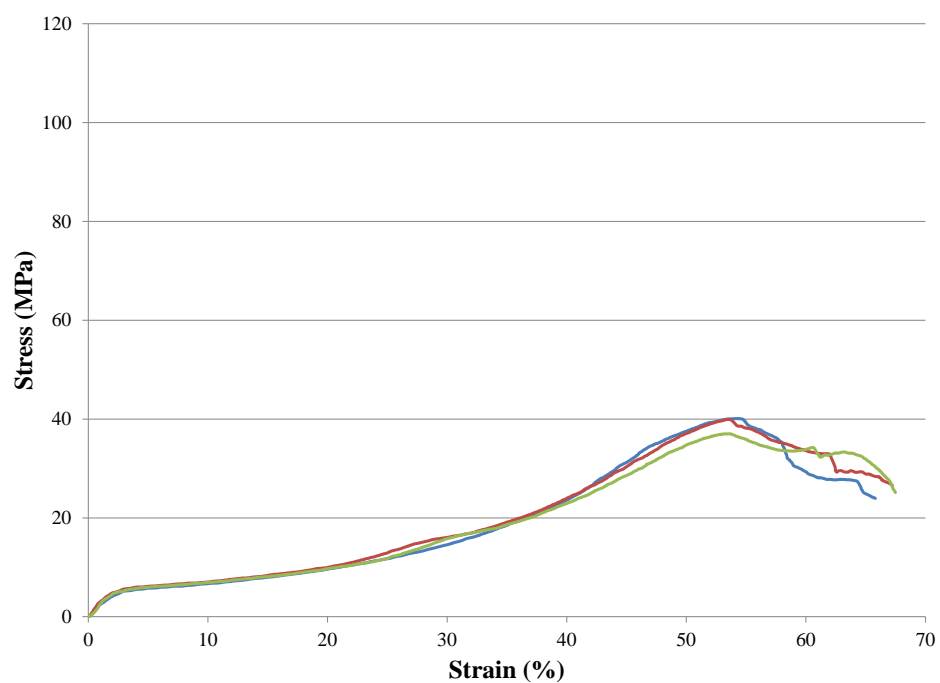
Fig. 9   Typical stress-strain curves for JA2 at a rate of ~100 s⁻¹ obtained at 50 °C
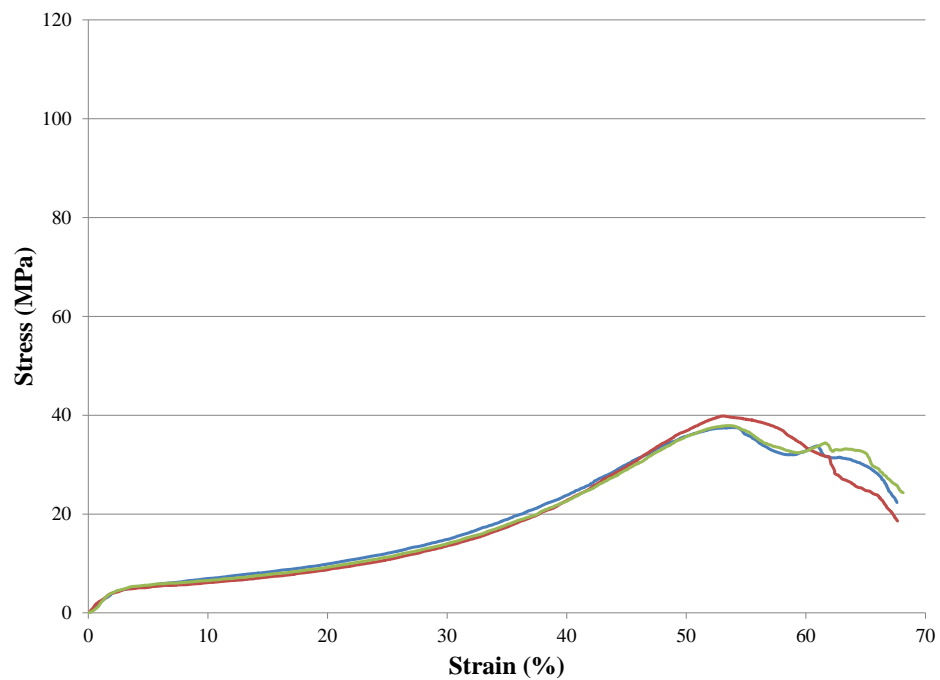
Fig. 10   Typical stress-strain curves for JA2 at a rate of ~100 s⁻¹ obtained at 40 °C
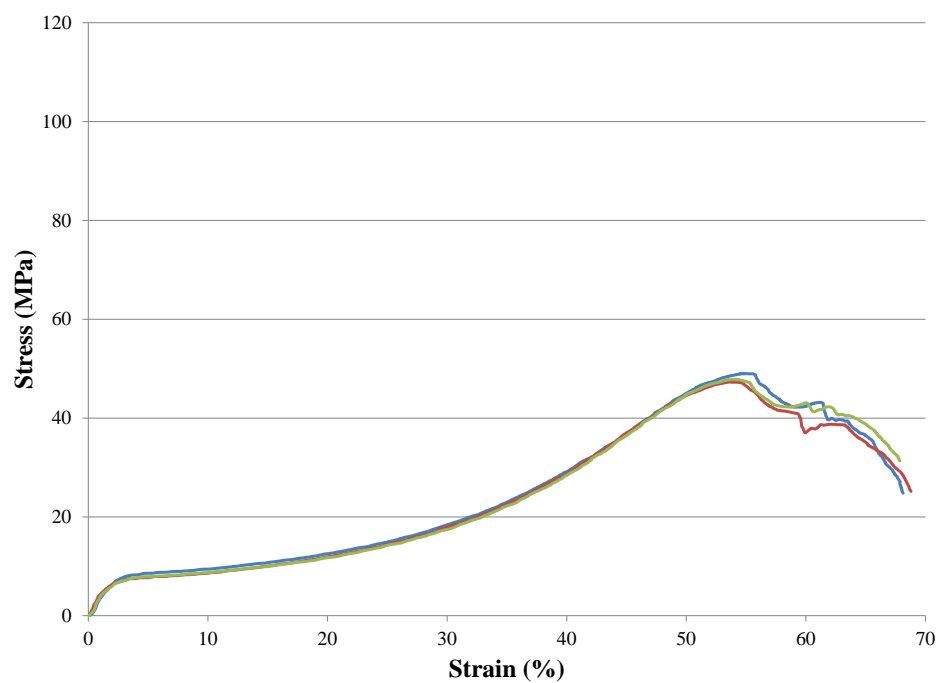
Fig. 11   Typical stress-strain curves for JA2 at a rate of ~100 s⁻¹ obtained at 30 °C
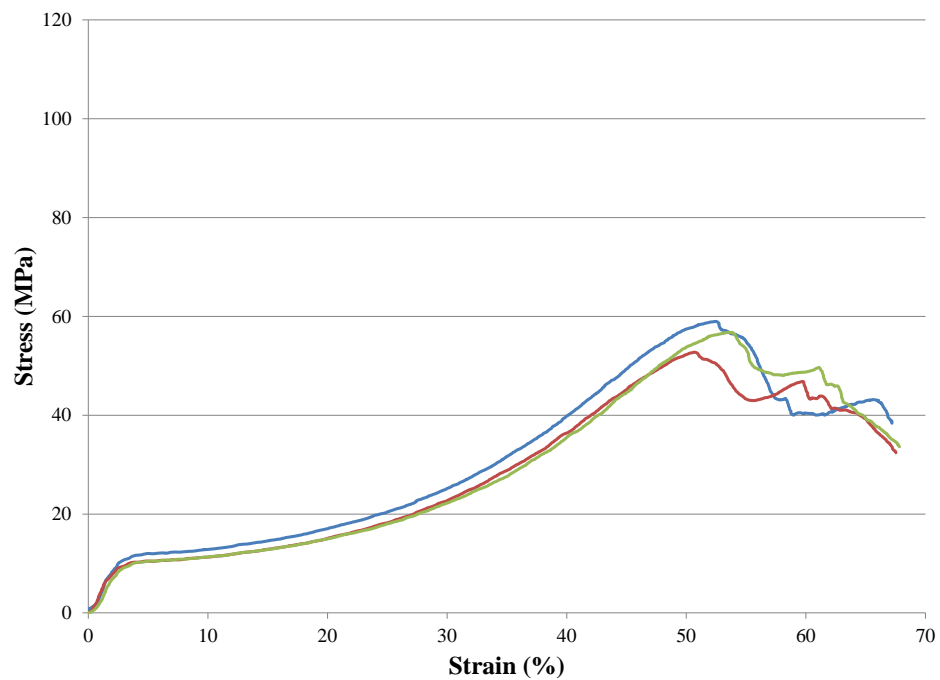
Fig. 12   Typical stress-strain curves for JA2 at a rate of ~100 s^{-1} obtained at 20 °C
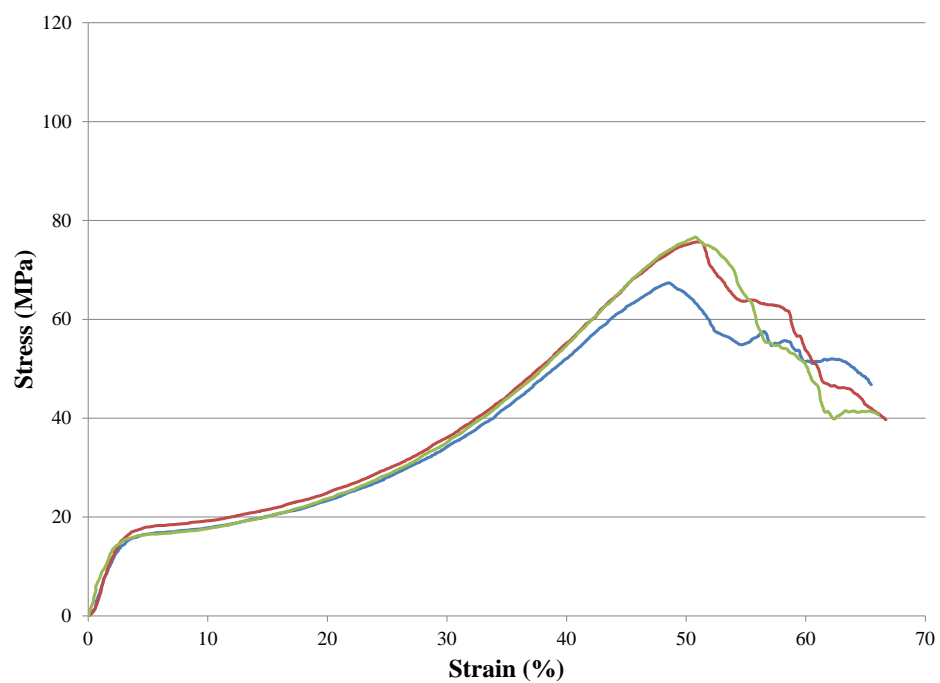
Fig. 13   Typical stress-strain curves for JA2 at a rate of ~100 s^{-1} obtained at 10 °C
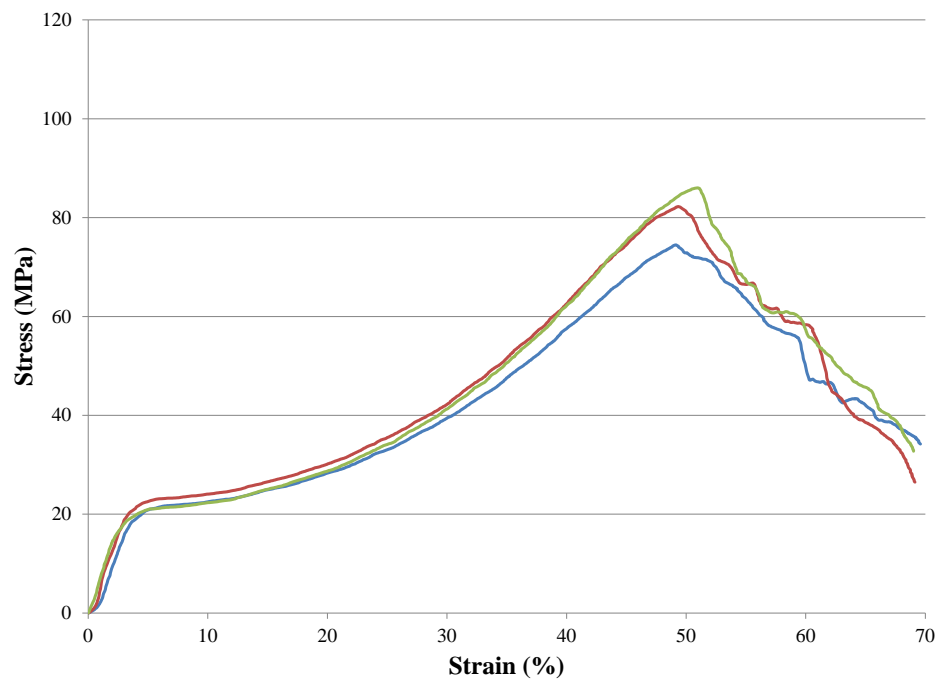
Fig. 14   Typical stress-strain curves for JA2 at a rate of ~100 s^{-1} obtained at 0 °C
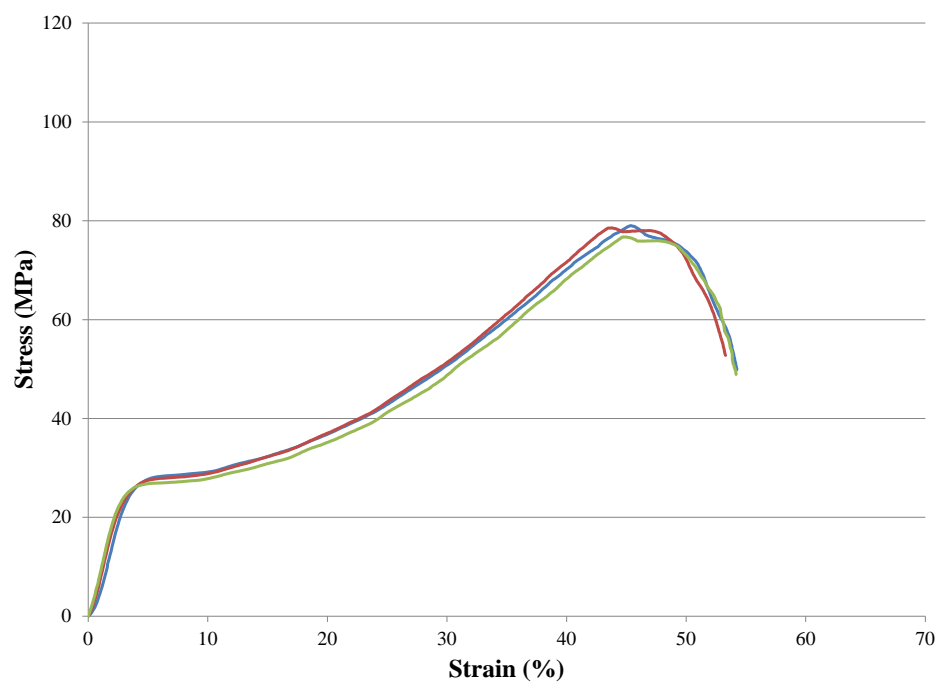
Fig. 15   Typical stress-strain curves for JA2 at a rate of ~100 s^{-1} obtained at –10 °C
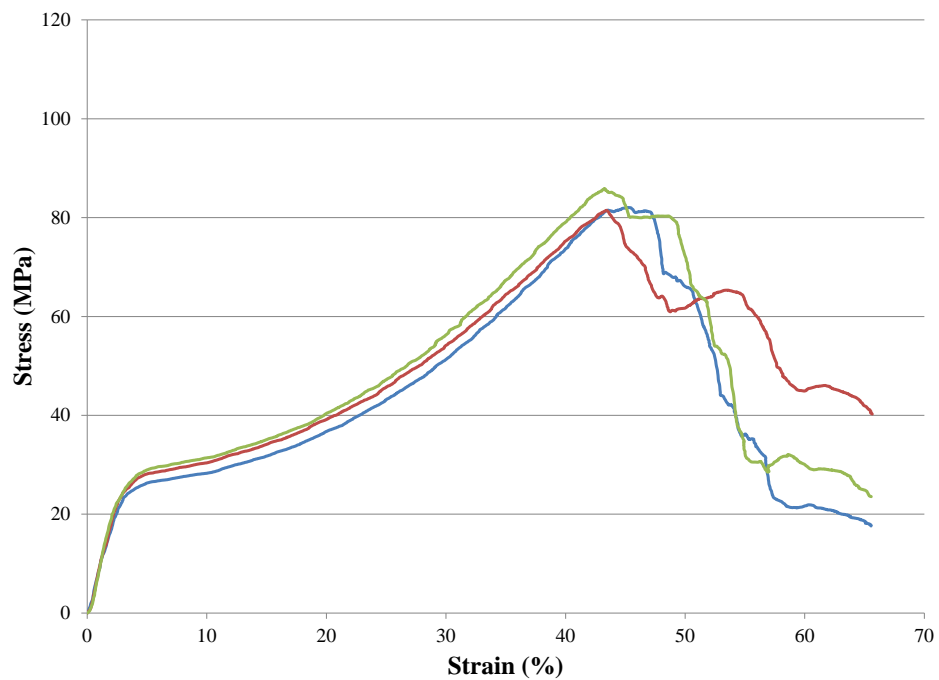
Fig. 16 Typical stress-strain curves for JA2 at a rate of ~100 s^{-1} obtained at –20 °C
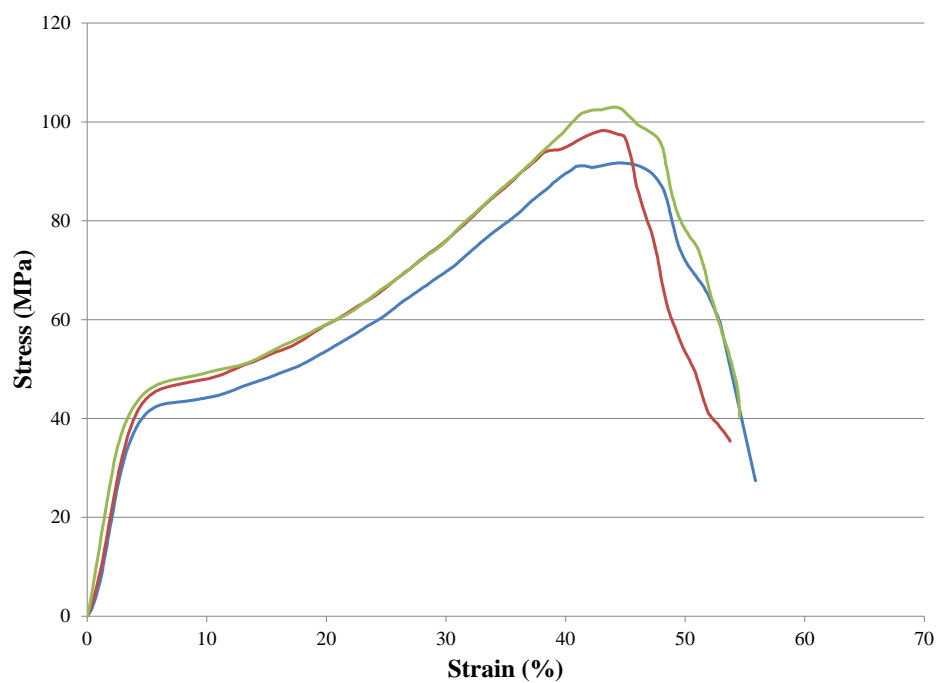
Fig. 17 Typical stress-strain curves for JA2 at a rate of ~100 s^{-1} obtained at –30 °C
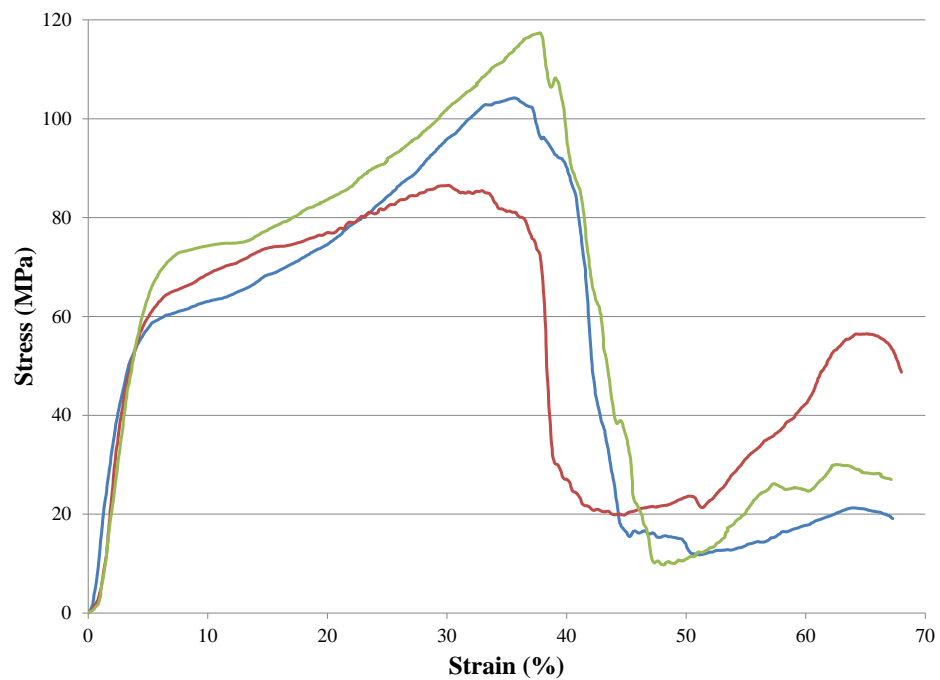
Fig. 18 Typical stress-strain curves for JA2 at a rate of ~100 s⁻¹ obtained at –40 °C
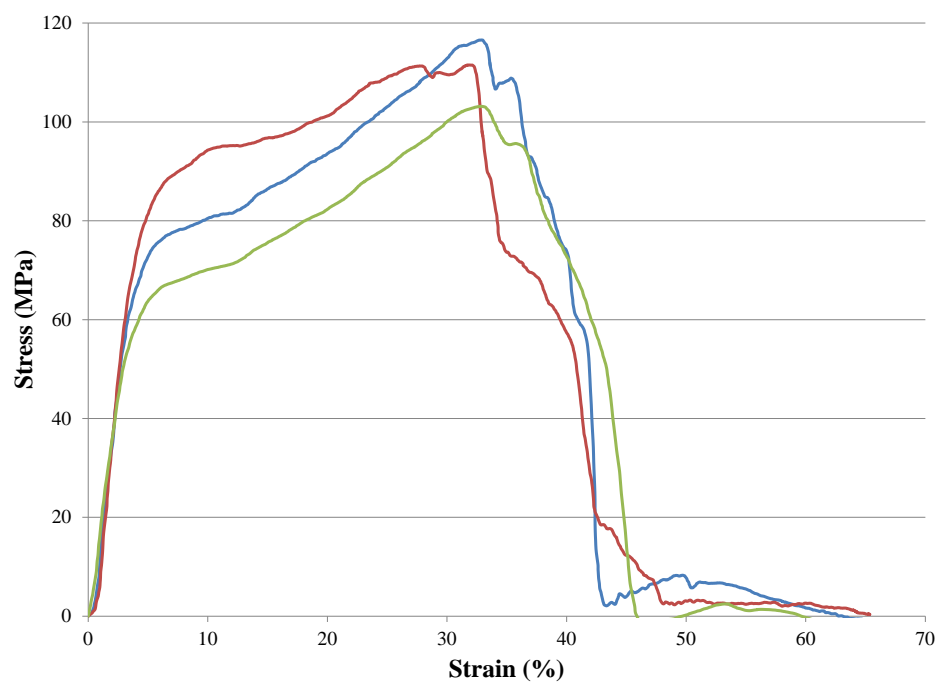
Fig. 19 Typical stress-strain curves for JA2 at a rate of ~100 s⁻¹ obtained at –50 °C

The compressive (Young's) modulus is defined as the slope of the linear region (Fig. 20) of the stress-strain curves in Figs. 6–19 as the stress increases from zero to the maximum supported stress. This region always occurs prior to the yield point (Fig. 20). In the case of JA2, the sample begins to yield at stresses slightly higher than those in the linear region where the compressive (Young's) modulus is defined. Without a local maximum to unambiguously define an apparent yield point,[12–15] locating the yield point is rather tenuous. The method of second derivative[16] also was used to locate the yield point.
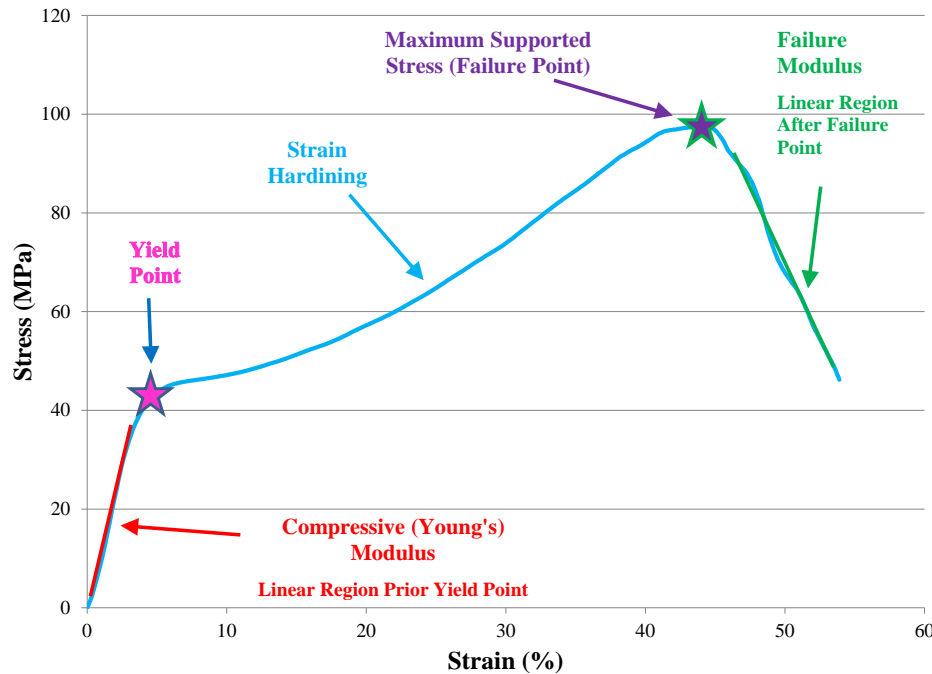
Fig. 20   Graphical depiction of data used to determine Young's modulus, yield point, failure point, and the failure modulus on a typical JA2 stress-strain curve

As JA2 yields, it supports increasing stress by strain hardening (Fig. 20) until the maximum supported stress is attained. After the maximum supported stress (defined as the point at which stress-reducing failure commences) is reached, the specimen can only support reduced levels of stress as the strain continues to increase. In this region of the stress-strain curve, the combination of all stress-reducing modes indicates that the specimen's structural integrity is compromised in some fashion and "failure" is occurring. The slope of the linear portion of this region of the stress-strain curve is defined to be the failure modulus (Fig. 20). Typically, the slope of the failure modulus is negative and indicative of failure modes reducing the applied stress in the specimen. As the modulus becomes more negative (larger in magnitude in the negative direction), the specimen exhibits increasingly brittle behavior. If the propellant is too brittle, the propellant can fracture in an unprogrammed fashion during a gun firing. This fracturing can

produce an unprogrammed increase in surface area of the propellant, which can produce an undesirable increase in burning rate and gaseous mass production. The increase in gaseous mass production can influence the interior ballistic cycle of the gun firing and adversely affect the performance, accuracy, and ultimately the life cycle of the gun itself.

The following Table contains the sample-averaged temperature-dependent Young's and failure moduli as obtained in this study. The table also delineates the averaged yield stress and averaged maximum supported (failure) stress at each temperature with its accompanying strain. A full analysis of this data is beyond the scope of this report and will be produced at a later date.[17]

Table. Averaged mechanical property parameters of JA2 7-perforation grain undergoing uniaxial compression at a rate of ~100 s^{-1} over a temperature range from –50 to 80 °C derived from Figs. 6–19 (measurement error of last significant digit in parentheses)

Temp. (°C)	Failure Stress (MPa)	Failure Strain (%)	Failure Modulus (GPa)	Young's Modulus (GPa)	Yield Stress (MPa)	Yield Strain (%)	Yield Strain by 2nd Derivative (%)
80	21(3)	42(4)	–0.150(5)	<0.01	<0.1	<0.5	ID[a]
70	26(5)	49(2)	–0.15(1)	<0.01	<0.1	<0.5	ID[a]
60	33(3)	52.4(7)	–0.6(2)	0.17(2)	4(2)	3(1)	1.5(5)
50	39(2)	53.6(4)	–0.45(3)	0.33(2)	5.2(5)	2.6(3)	2.7(7)
40	38.4(9)	53.4(3)	–0.41(2)	0.25(5)	4.2(4)	2.1(3)	2.1(2)
30	48.0(7)	54(1)	–0.54(4)	0.48(2)	6.5(4)	2.1(1)	2.8(8)
20	56(3)	52(2)	–0.40(9)	0.56(4)	9.3(7)	2.6(2)	2.2(6)
10	76.1(5)	50(2)	–0.34(7)	0.8(1)	14.7(5)	2.8(4)	3(1)
0	84(2)	49.8(7)	–0.5(2)	0.69(6)	19(1)	3.4(4)	2.7(5)
–10	78(1)	44.6(9)	–0.73(1)	0.95(2)	25.5(5)	3.5(3)	2.5(5)
–20	83(2)	44.0(7)	–1.2(4)	1.0(1)	26(2)	4(1)	2.6(2)
–30	98(6)	43.9(7)	–1.0(2)	1.36(4)	46(4)	4.5(5)	2(1)
–40	111(7)	37(1)	–3(2)	2.1(2)	64(8)	6(1)	3(1)
–50	110(7)	32.5(8)	–3(1)	2.4(1)	80(10)	5(1)	2.4(6)

[a]ID = indeterminate

After the compression event, the impact bell was raised and the propellant was recovered from the SHT stage and visually imaged as a group executed at the same temperature. Figures 21–34 show, respectively, the recovered propellant fragment(s) for the stress/strain curves in Figs. 6–19. The view is from the impact bell. As noted in the Table, the failure modulus becomes increasingly more negative as the temperature decreases. This trend is mirrored in Figs. 21–34 with an increased number of fragments as the temperature is decreased.
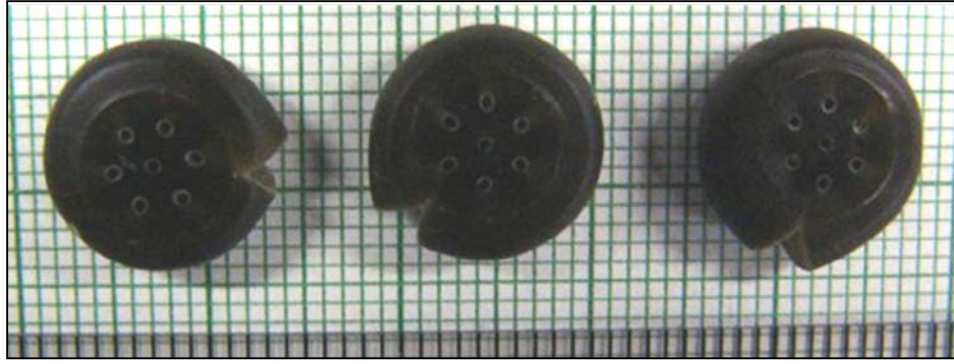
Fig. 21   Postcompression image of JA2 grain samples at a rate of ~100 s^{-1} obtained at 80 °C, scale in millimeters
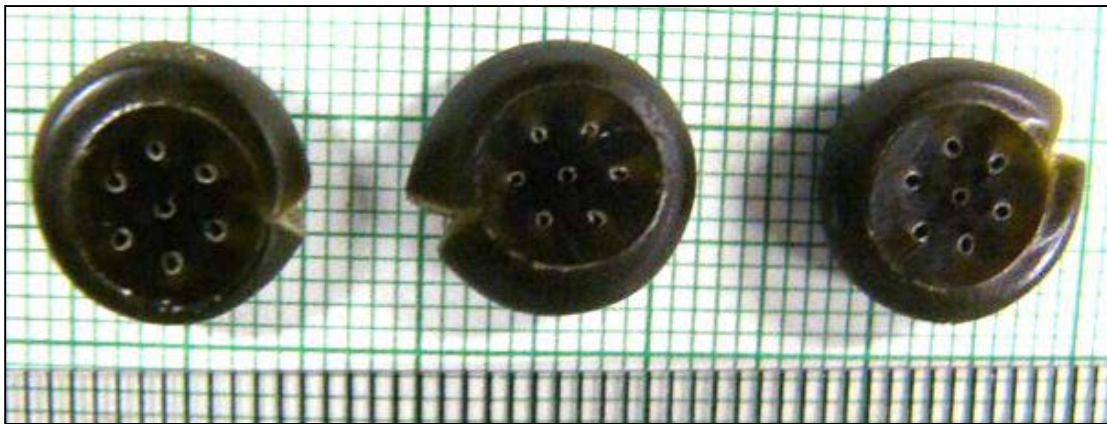
Fig. 22   Postcompression image of JA2 grain samples at a rate of ~100 s^{-1} obtained at 70 °C, scale in millimeters
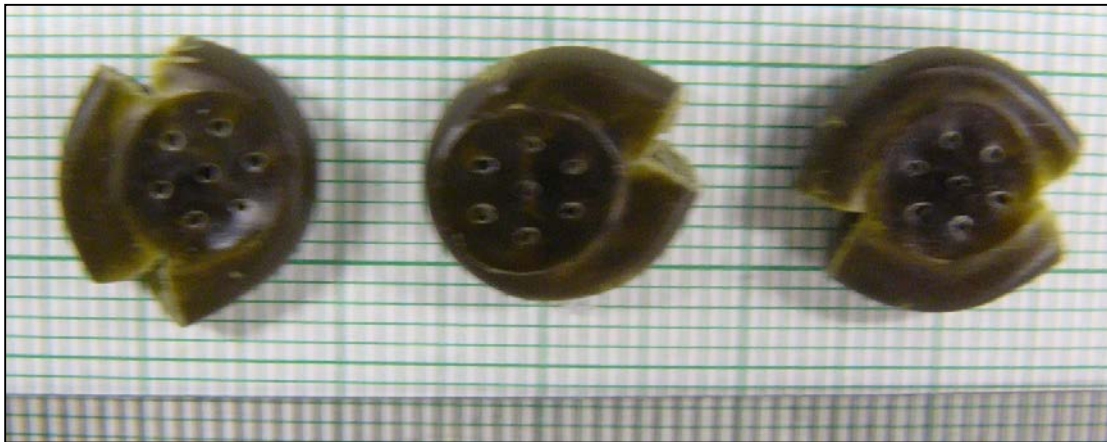
Fig. 23   Postcompression image of JA2 grain samples at a rate of ~100 s^{-1} obtained at 60 °C, scale in millimeters
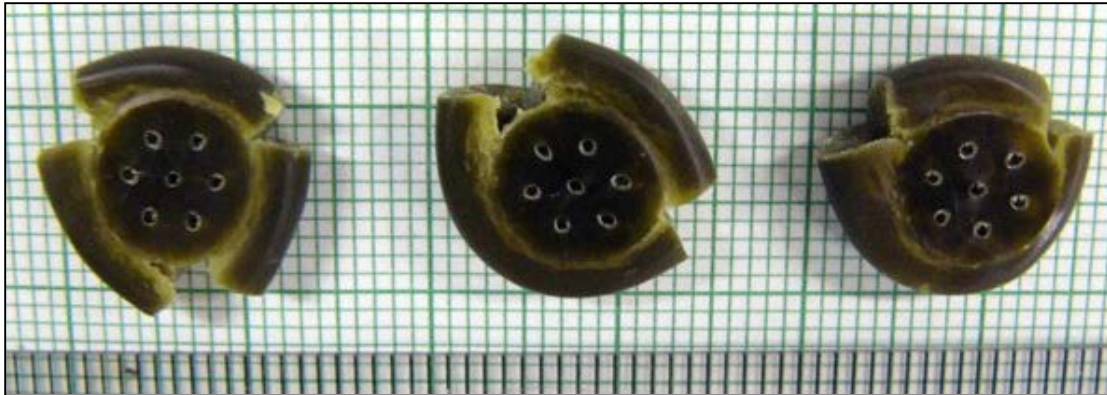
Fig. 24 **Postcompression image of JA2 grain samples at a rate of ~100 s⁻¹ obtained at 50 °C, scale in millimieters**
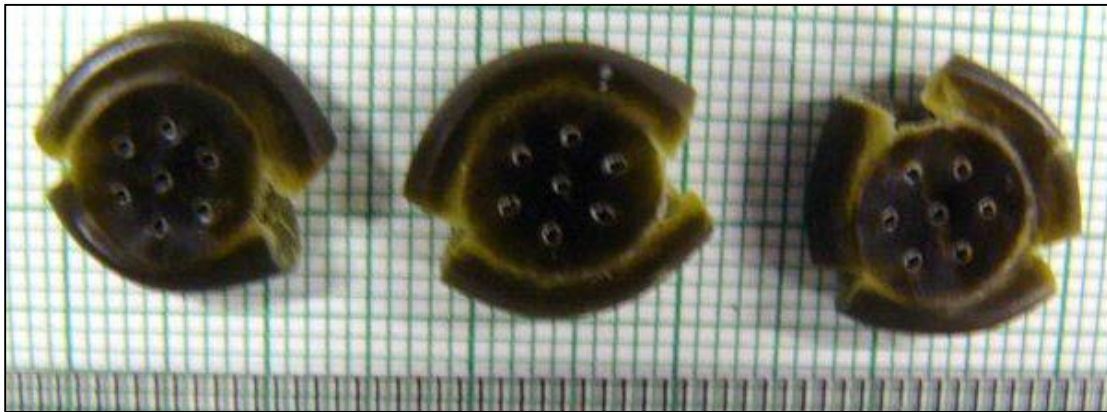
Fig. 25 **Postcompression image of JA2 grain samples at a rate of ~100 s⁻¹ obtained at 40 °C, scale in millimeters**
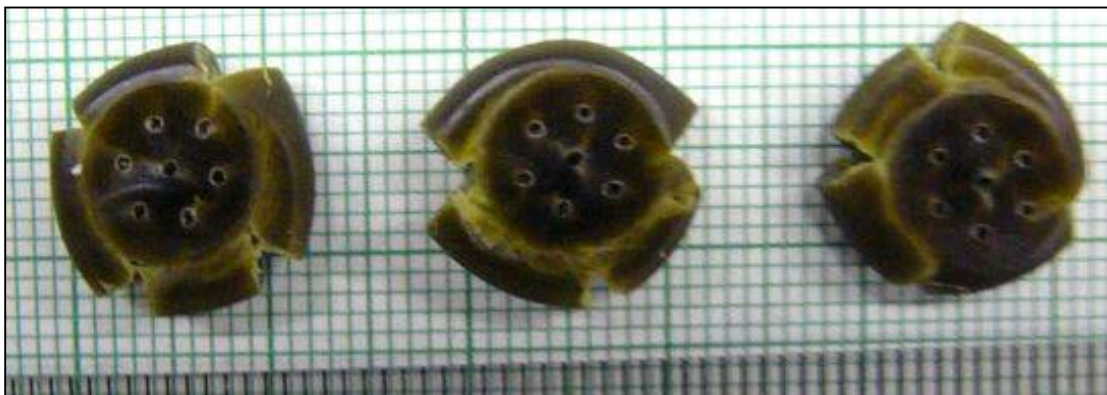
Fig. 26 **Postcompression image of JA2 grain samples at a rate of ~100 s⁻¹ obtained at 30 °C, scale in millimeters**
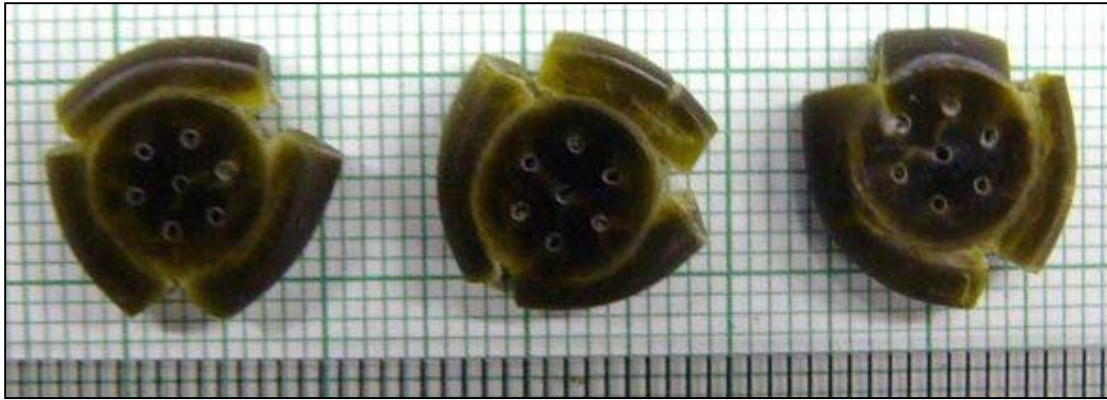
Fig. 27 Postcompression image of JA2 grain samples at a rate of ~100 s^{-1} obtained at 20 °C, scale in millimeters
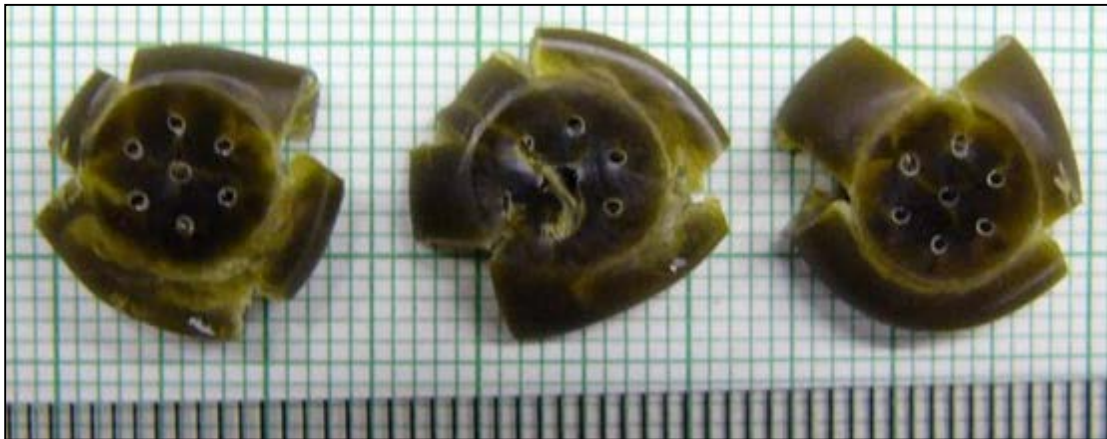
Fig. 28 Postcompression image of JA2 grain samples at a rate of ~100 s^{-1} obtained at 10 °C, scale in millimeters
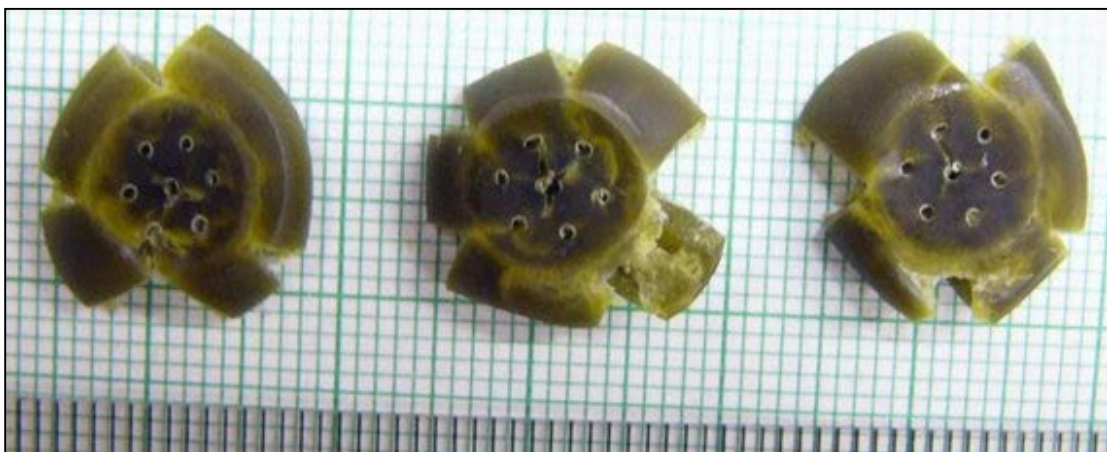
Fig. 29 Postcompression image of JA2 grain samples at a rate of ~100 s^{-1} obtained at 0 °C, scale in millimeters

16
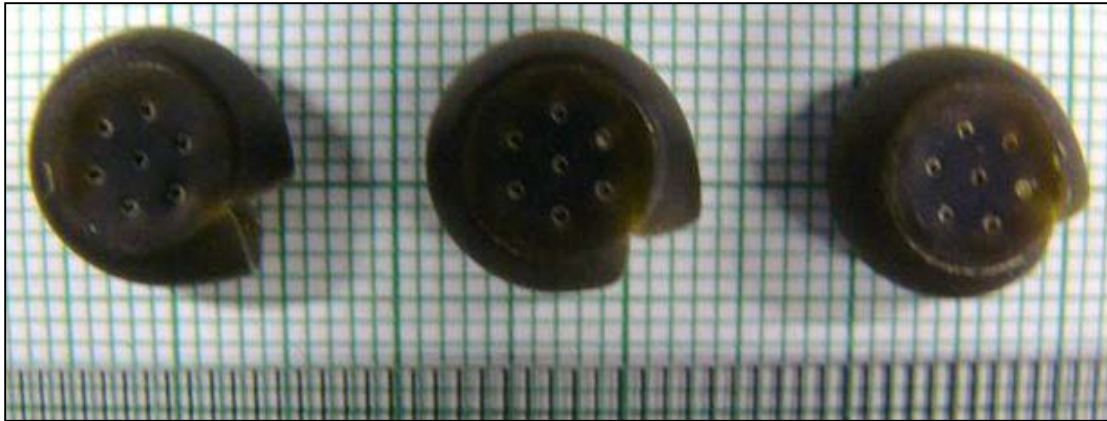
Fig. 30 **Postcompression image of JA2 grain samples at a rate of ~100 s⁻¹ obtained at –10 °C, scale in millimeters**
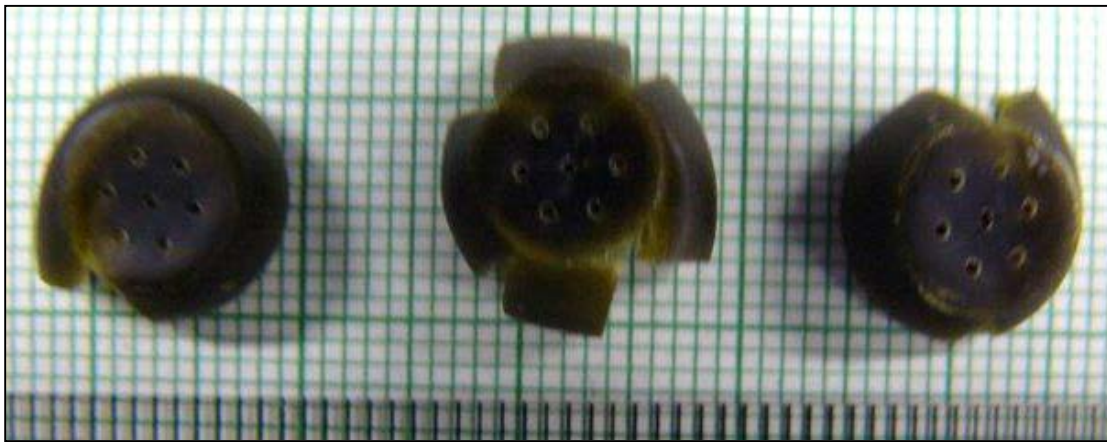
Fig. 31 **Postcompression image of JA2 grain samples at a rate of ~100 s⁻¹ obtained at –20 °C, scale in millimeters**
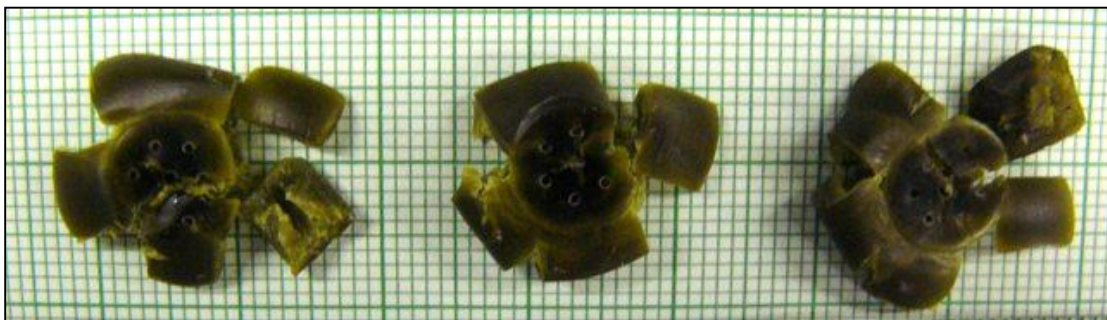
Fig. 32 **Postcompression image of JA2 grain samples at a rate of ~100 s⁻¹ obtained at –30 °C, scale in millimeters**
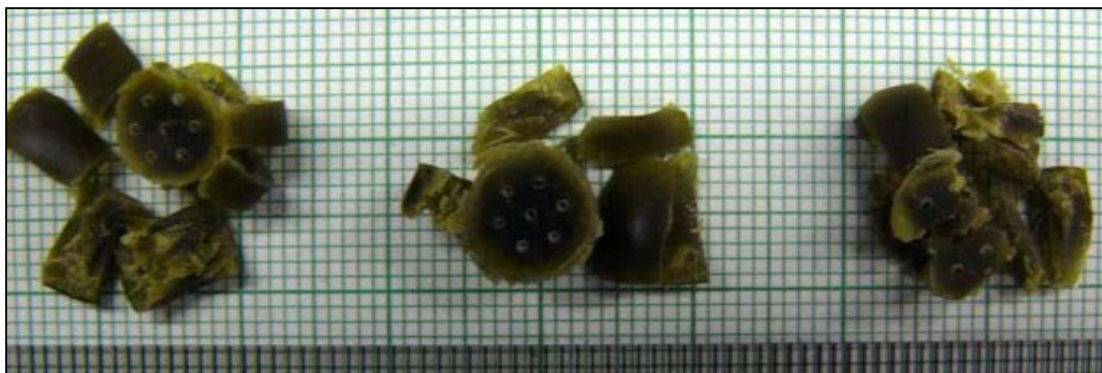
Fig. 33 Postcompression image of JA2 grain samples at a rate of ~100 s^{-1} obtained at –40 °C, scale in millimeters

Fig. 34 Postcompression image of JA2 grain samples at a rate of ~100 s^{-1} obtained at –50 °C, scale in millimeters

After the compressed samples were recovered from the platen, the samples were prepared for electron microscopy. Nearly whole grains (i.e., Figs. 21–32) were chilled over liquid nitrogen for 30 min and cold-cleaved. The target for cold-cleaving was to create a cross section containing up to 3 perforations. The cold-cleave process minimally disturbs the shape and morphology of the sample for internal cross-section examination. Samples such as in Figs. 33 and 34 did not require cold cleaving for acquiring internal cross-sectional information.

The SEM images for the grain cross sections were assembled as a panorama view of the cross sections so that both sides of the cold-cleaved sample could be viewed when possible. Some of the images in Figs. 35–48 show scrape marks from the cleaving blade, but sufficient undisturbed areas are present for the analysis required in this study.
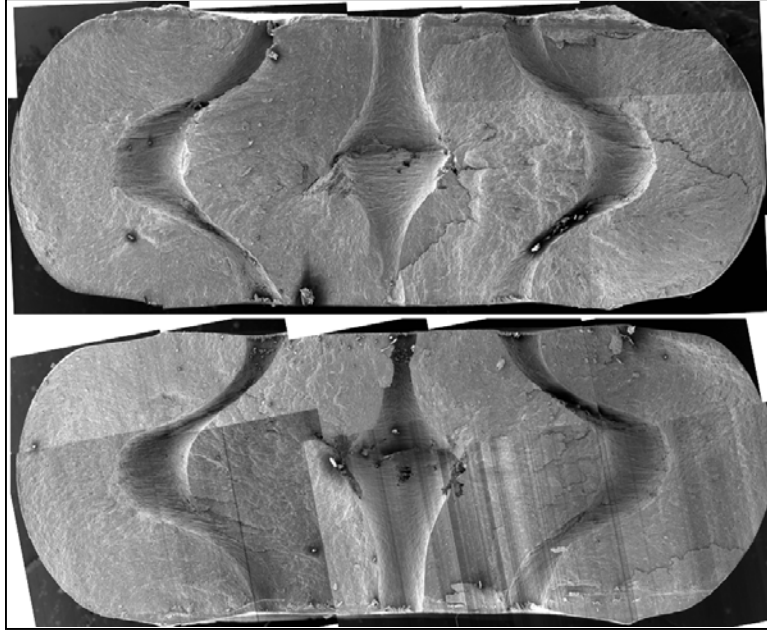
Fig. 35   SEM panorama of postcompression JA2 grain sample (uniaxially compressed at a rate of ~100 s⁻¹, 80 °C, and strain greater than 40%), 50× magnification
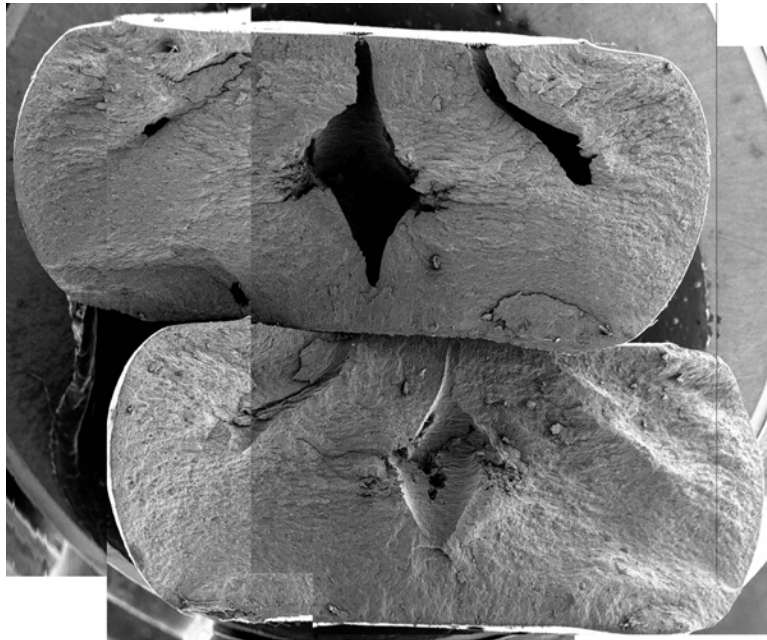
Fig. 36   SEM panorama of postcompression JA2 grain sample (uniaxially compressed at a rate of ~100 s⁻¹, 70 °C, and strain greater than 40%), 10× magnification
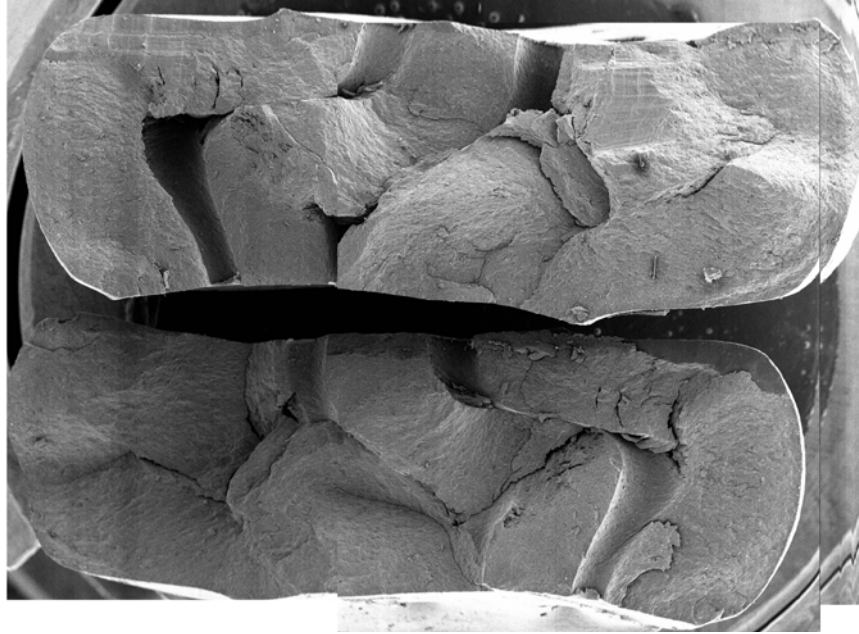
Fig. 37   SEM panorama of postcompression JA2 grain sample (uniaxially compressed at a rate of ~100 s^{-1}, 60 °C, and strain greater than 40%), 50× magnification
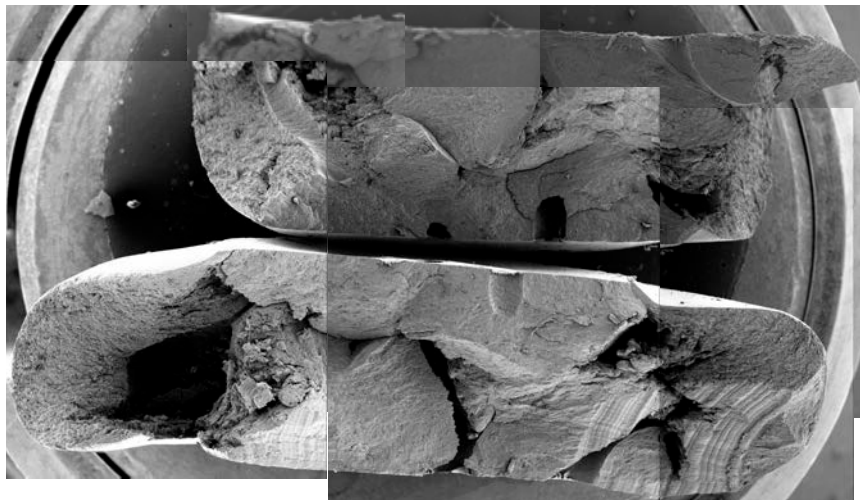
Fig. 38   SEM panorama of postcompression JA2 grain sample (uniaxially compressed at a rate of ~100 s^{-1}, 50 °C, and strain greater than 40%), 10× magnification
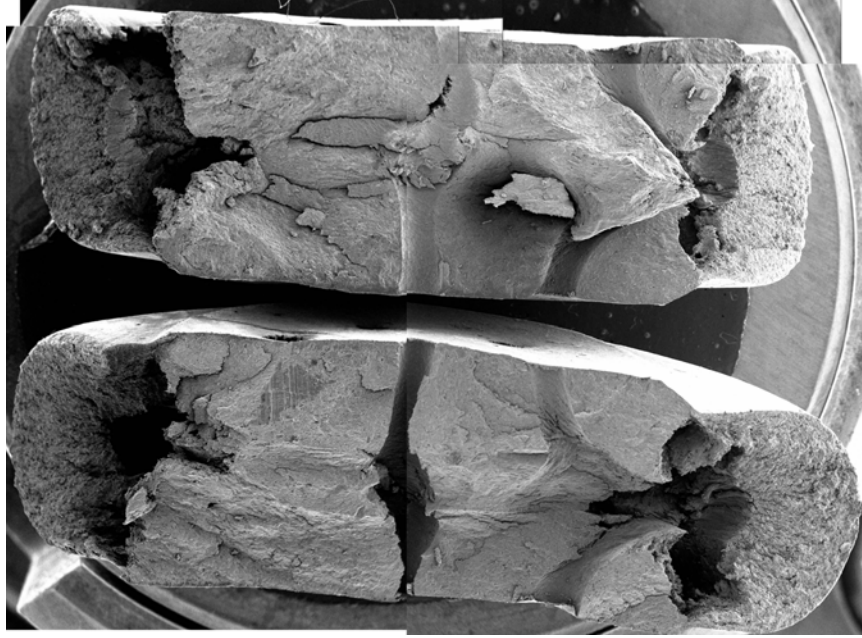
Fig. 39   SEM panorama of postcompression JA2 grain sample (uniaxially compressed at a rate of ~100 s⁻¹, 40 °C, and strain greater than 40%), 10× magnification
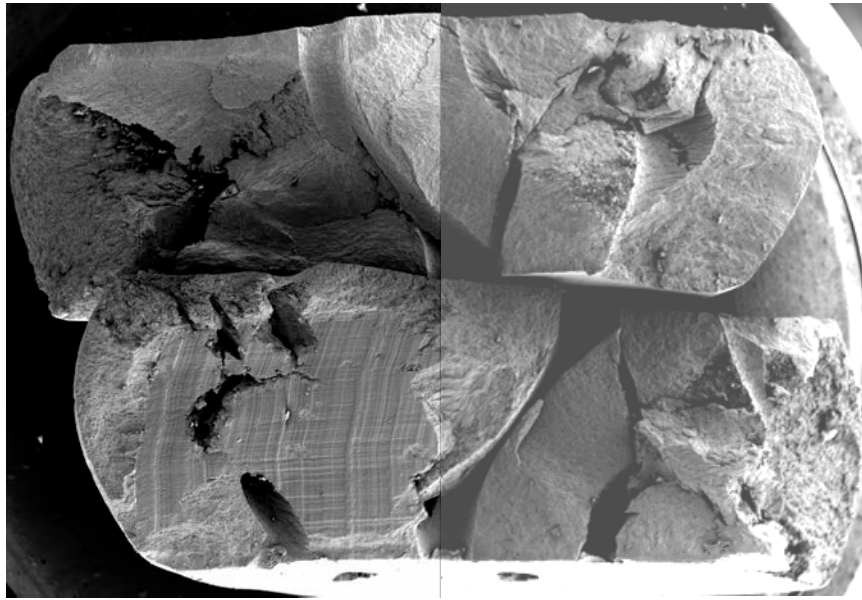
Fig. 40   SEM panorama of postcompression JA2 grain sample (uniaxially compressed at a rate of ~100 s⁻¹, 30 °C, and strain greater than 40%), 10× magnification
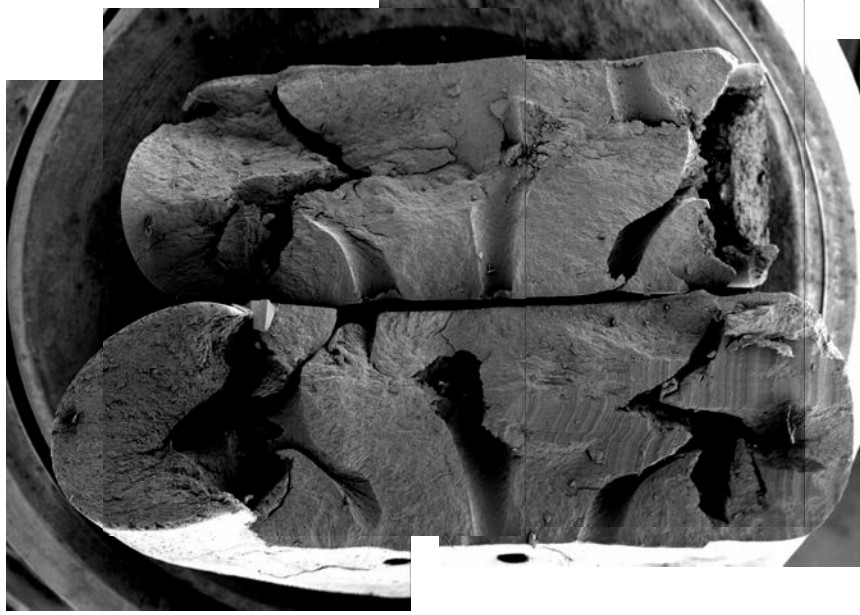
Fig. 41   SEM panorama of postcompression JA2 grain sample (uniaxially compressed at a rate of ~100 s^{-1}, 20 °C, and strain greater than 40%), 10× magnification
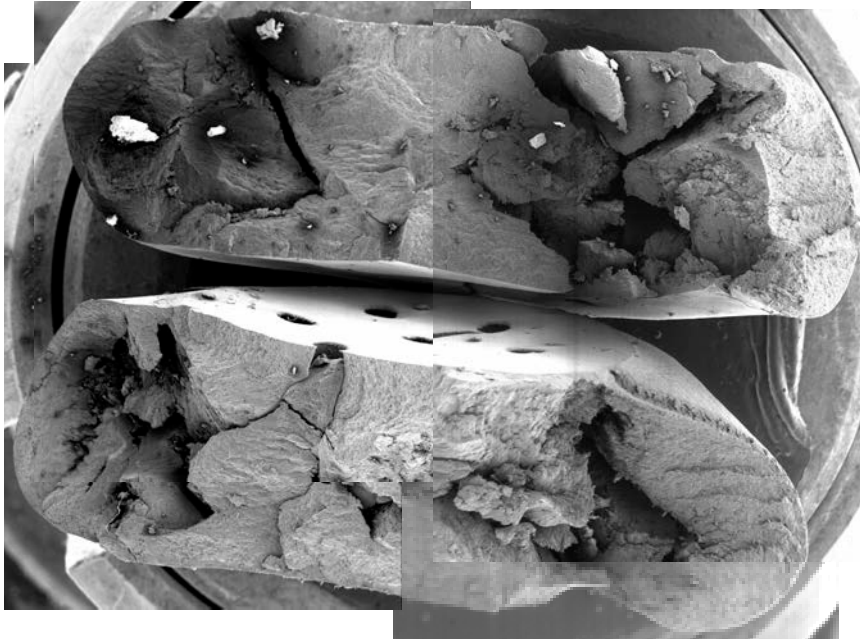
Fig. 42   SEM panorama of postcompression JA2 grain sample (uniaxially compressed at a rate of ~100 s^{-1}, 10 °C, and strain greater than 40%), 10× magnification
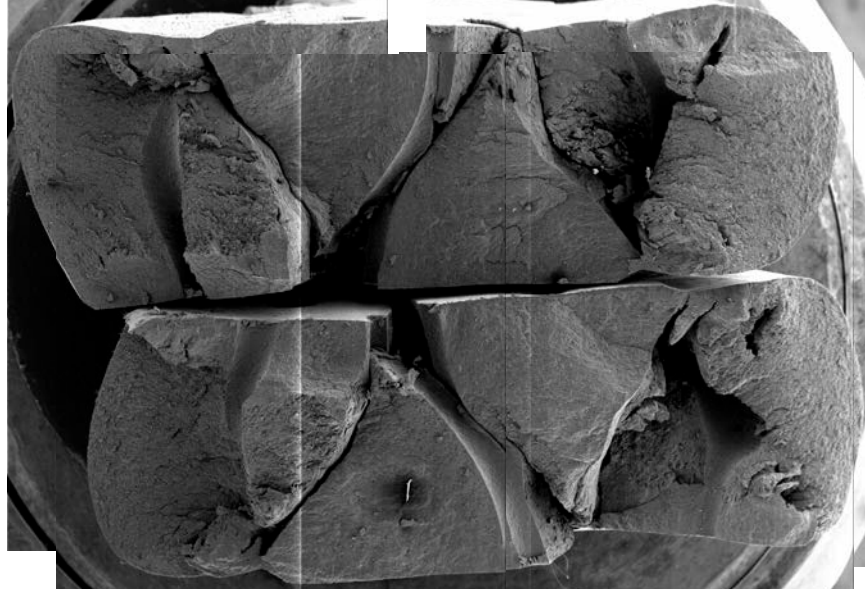
Fig. 43   SEM panorama of postcompression JA2 grain sample (uniaxially compressed at a rate of ~100 s⁻¹, 0 °C, and strain greater than 40%), 10× magnification
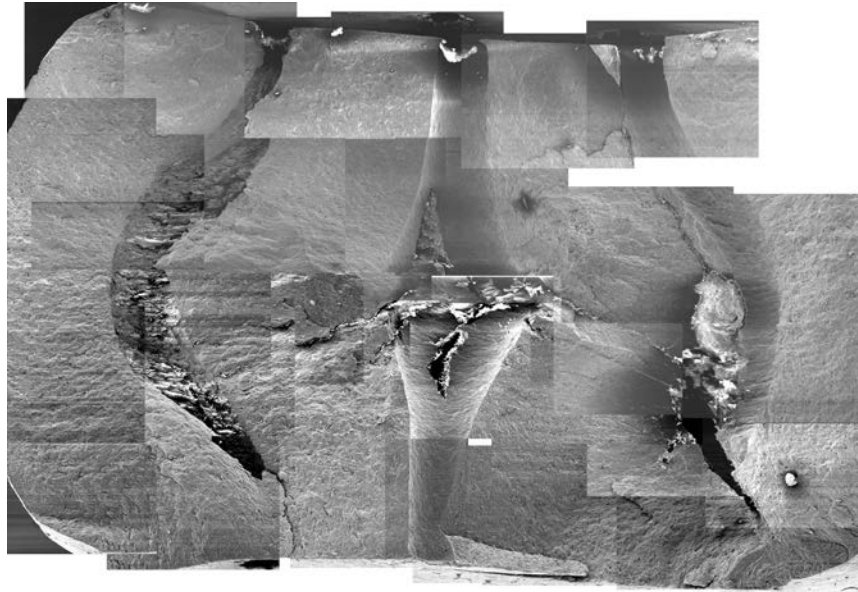
Fig. 44   SEM panorama of postcompression JA2 grain sample (uniaxially compressed at a rate of ~100 s⁻¹, –10 °C, and strain greater than 40%), 50× magnification
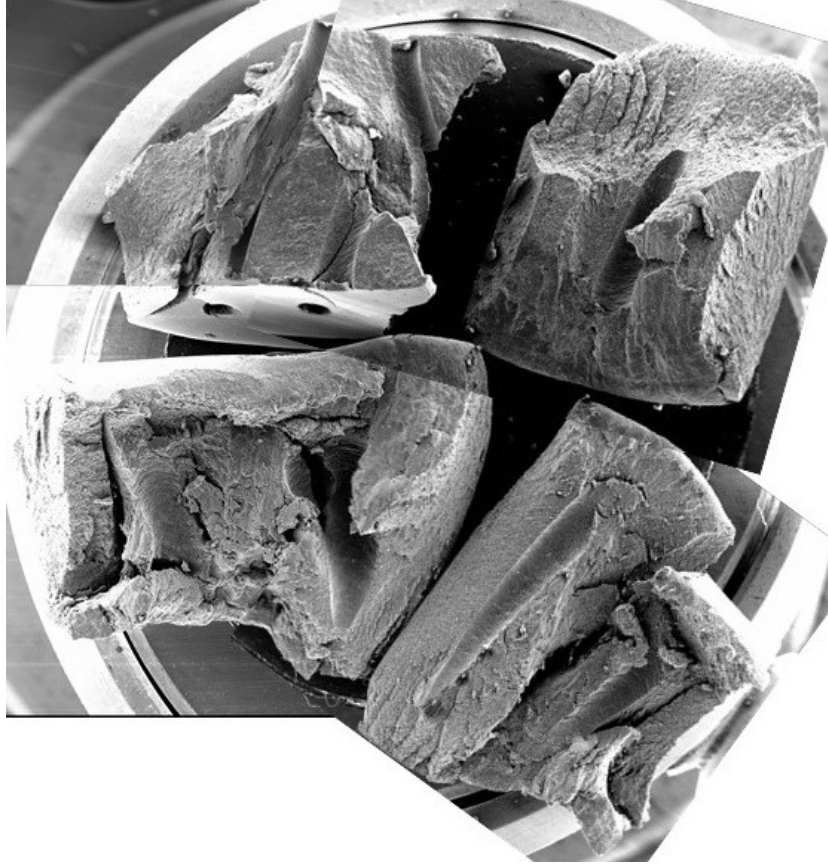
Fig. 45   SEM panorama of postcompression JA2 grain sample (uniaxially compressed at a rate of ~100 s^{-1}, –20 °C, and strain greater than 40%), 50× magnification
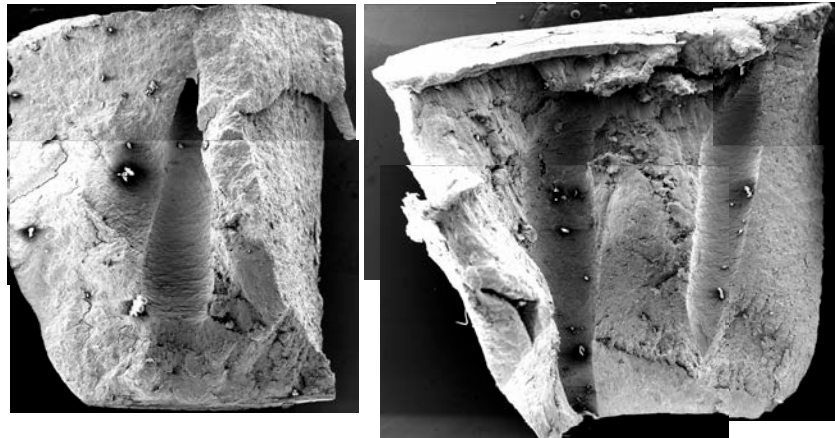
Fig. 46   SEM panorama of postcompression JA2 grain sample (uniaxially compressed at a rate of ~100 s^{-1}, –30 °C, and strain greater than 40%), 50× magnification

Fig. 47   SEM panorama of postcompression JA2 grain sample (uniaxially compressed at a rate of ~100 s^{-1}, –40 °C, and strain greater than 40%), 50× magnification

Fig. 48   SEM panorama of postcompression JA2 grain sample (uniaxially compressed at a rate of ~100 s^{-1}, –50 °C, and strain greater than 40%), 10× magnification

All of the samples in Figs. 35–48 were compressed to a strain greater than the failure point. Therefore, all of the samples showed failure damage in addition to deformation damage as functions of temperature. At the higher temperatures (Figs. 35 and 36), the deformation damage was mostly barrel expansion with little internal failure damage. The perforations were still open end to end, but were significantly enlarged mid-sample. Internal failure damage was mostly enlargement of the central perforation with a single fracture on the exterior hoop of the sample (Figs. 21 and 22). This deformation demonstrated a viscous flow over much of the strain range. Another indicator of the possibility of viscous flow are the greatly reduced Young's moduli in the Table for these temperatures.

As the temperature decreased (Figs. 37–44), the Young's moduli in the Table increased, the failure modulus became more negative, and internal fractures became more evident. While some flow was evident in the expansion of the perforations, internal fractures and voids formed with more surface area generation. JA2 at these temperatures is definitely more rigid and brittle than at above 60 °C.

Below –10 °C, JA2 rapidly becomes more rigid and brittle. Figure 45 shows very little enlargement of the perforations and shows extensive fractures. These factors indicate that the temperature may be approaching a glass transition temperature (T_g). Another study using a different technique has shown a possible T_g for JA2 near –21 °C.[18] Below –30 °C (Figs. 47 and 48), there appears to be only brittle fracture damage.

Because the strain in Figs. 21–34 and 35–48 was allowed to exceed the failure point, the postmortem examination of these samples shows only the ultimate damage experienced past the failure point. Examination of the stress-strain curves in Figs. 6–19 shows that if the strain were kept below 37% engineering strain, all of the samples would experience deformation below the failure point but not complete structural failure. Examination of the internal morphology then could reveal clues to the accumulating damage to the sample that would ultimately initiate the failure.

Figures 49–66 are SEM images obtained from samples at selected temperatures that were uniaxially compressed to approximately 35% strain. The samples were then cold-cleaved and examined. Figures 49–57 are images at 10× magnification and are useful for examining the gross deformation of the sample. Figures 58–66 are from the same samples as Figs. 49–57 but are obtained at a higher 50× magnification and show evidence of the damage accumulating as the JA2 work-hardened prior to the failure point.

Figures 49–52 show fairly smooth deformation along the axis of the sample. The most dilation damage occurred nearest the end of the sample that rested on the SHT stage. As the temperature decreased, the region of major dilation moved upward along the sample until it was approximately midway between the compression platens.

It is possible that this deformation is evidence of the pressure wave initiated by the impact of the impact bell on the sample as it reflected off of the opposite end of the sample and was reinforced by the continuing pressure from the still-moving impact bell. The viscosity of the JA2 would be the least in Fig. 49 and would be greater in Fig. 52. The increasing viscosity and stiffness of the sample as the temperature was decreased should shift the reinforcing region closer to the incoming pressure wave as shown in these figures.

Figure 54 (–20 °C) shows the rapid onset of less ductile behavior (an indicator of a possible T_g). The perforations show less barreling deformation and little dilation. The cold-cleave process also was not as clean, indicating that the resiliency of the sample was compromised during uniaxial compression and that random failure mode sites were present, which compromised the cold-cleave process. This behavior continued through Figs. 54–57 (temperatures down to –50 °C).

Figures 58–66 show higher magnified regions of the samples from Figs. 49–57. At 60 °C (Fig. 58), there were few microvoids formed; however, the small cracks that formed originated from the microvoids. Otherwise, not much damage was noted. At 40 °C (Fig. 59), more microvoids were noted as well as some larger void openings in the perforation region. At 20 °C (Fig. 60), more frequent and larger void openings in the perforation region were formed.

At 0 °C (Fig. 61), voids were larger and more frequent. Crack formation from void to void was evident as more cracks were formed. At –10 °C (Fig. 62), the cracks became longer as the crack tip progressed from void to void.

Below –20 °C (Figs. 63–66), voids were larger and more frequent. Crack propagation appeared to move from void to void with fewer extended cracks than at warmer temperatures. Fracture extending directly from void to void with an increasing number of voids with less material between voids should be less energy-intensive than solely crack-tip propagation.[19,20] The decreased failure strain and the larger magnitude of the failure modulus in the Table at temperatures below approximately –20 °C are indicative of this trend. The shape and number of fragments in Figs. 31–34 also indicate that the fracture process is more random and more efficient as the temperature was dropped below approximately –10 °C.
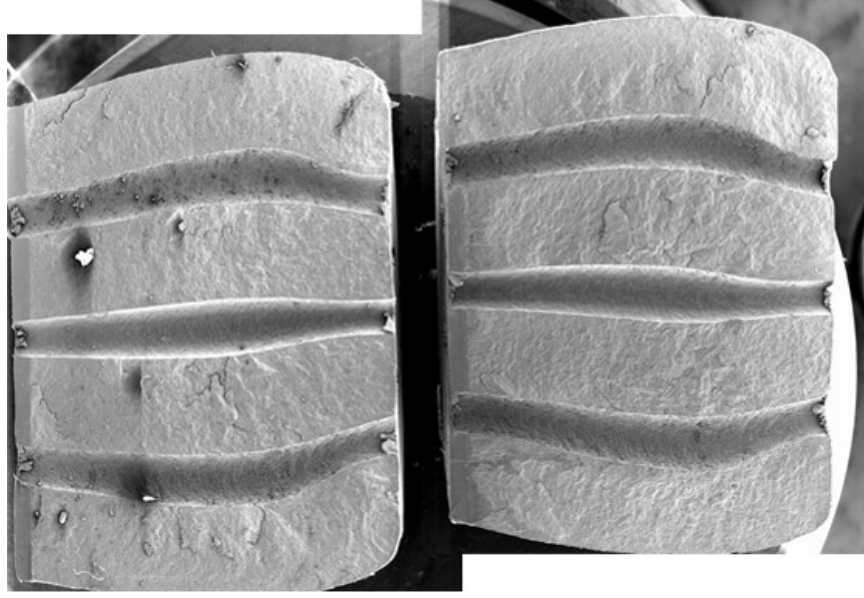
Fig. 49   SEM panorama of postcompression JA2 grain sample (uniaxially compressed at a rate of ~100 s^{-1}, 60 °C, and strain equal to 35%), 10× magnification
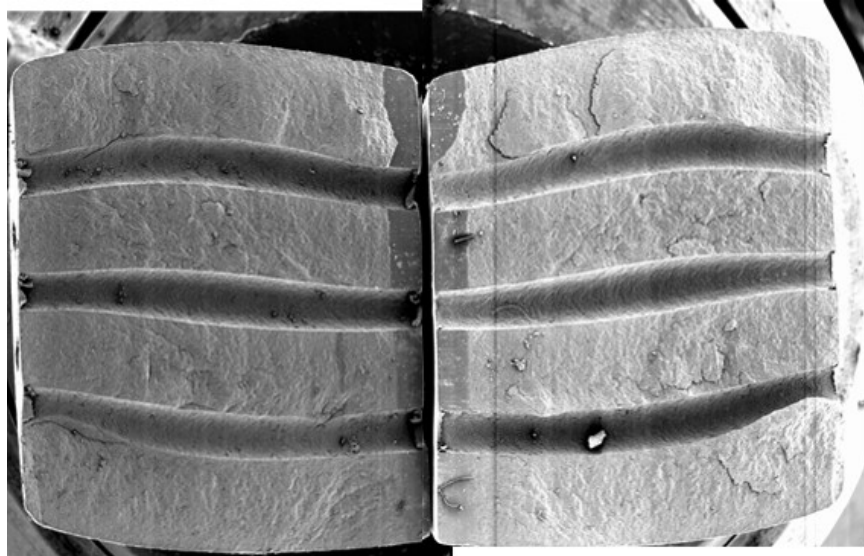
Fig. 50   SEM panorama of postcompression JA2 grain sample (uniaxially compressed at a rate of ~100 s^{-1}, 40 °C, and strain equal to 35%), 10× magnification
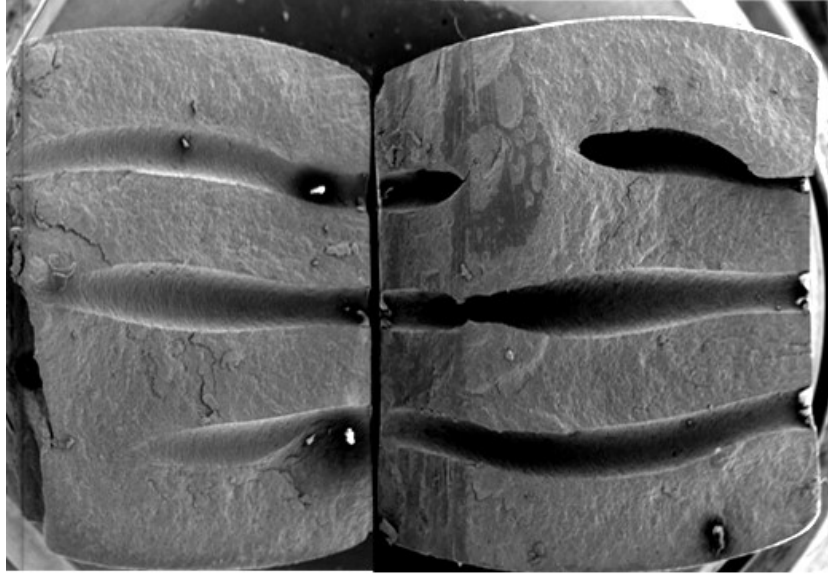
Fig. 51   SEM panorama of postcompression JA2 grain sample (uniaxially compressed at a rate of ~100 s^{-1}, 20 °C, and strain equal to 35%), 10× magnification
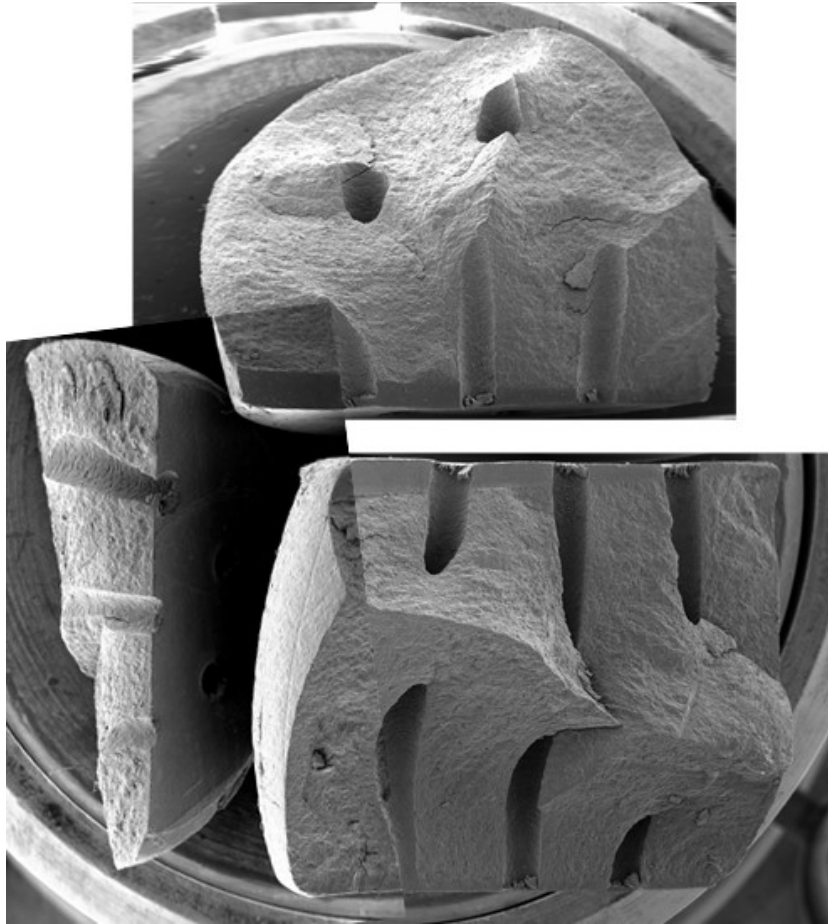
Fig. 52   SEM panorama of postcompression JA2 grain sample (uniaxially compressed at a rate of ~100 s^{-1}, 0 °C, and strain equal to 35%), 10× magnification
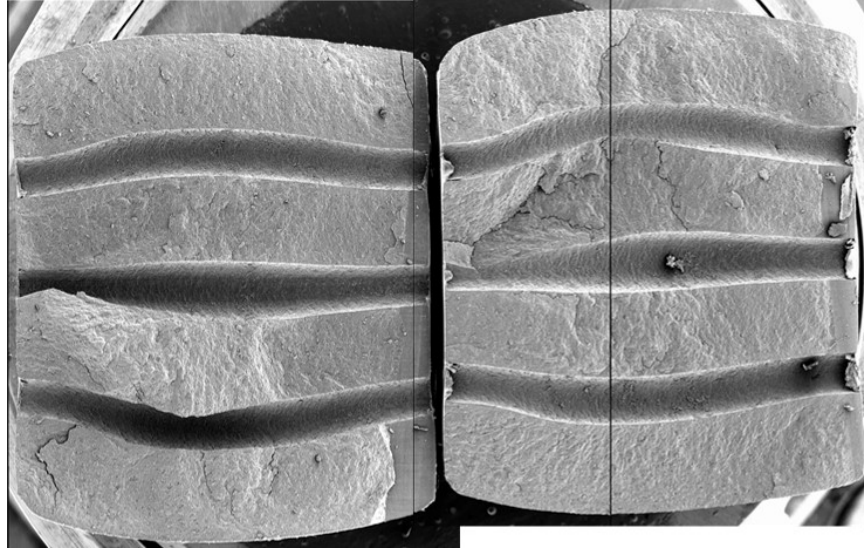
Fig. 53   SEM panorama of postcompression JA2 grain sample (uniaxially compressed at a rate of ~100 s⁻¹, –10 °C, and strain equal to 35%), 10× magnification
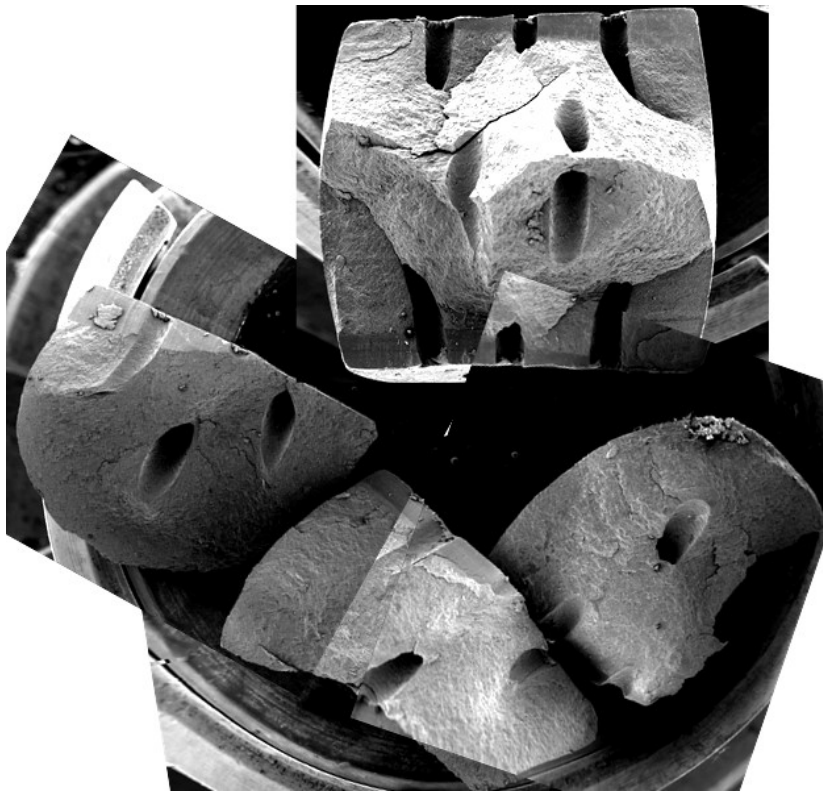
Fig. 54   SEM panorama of postcompression JA2 grain sample (uniaxially compressed at a rate of ~100 s⁻¹, –20 °C, and strain equal to 35%), 10× magnification
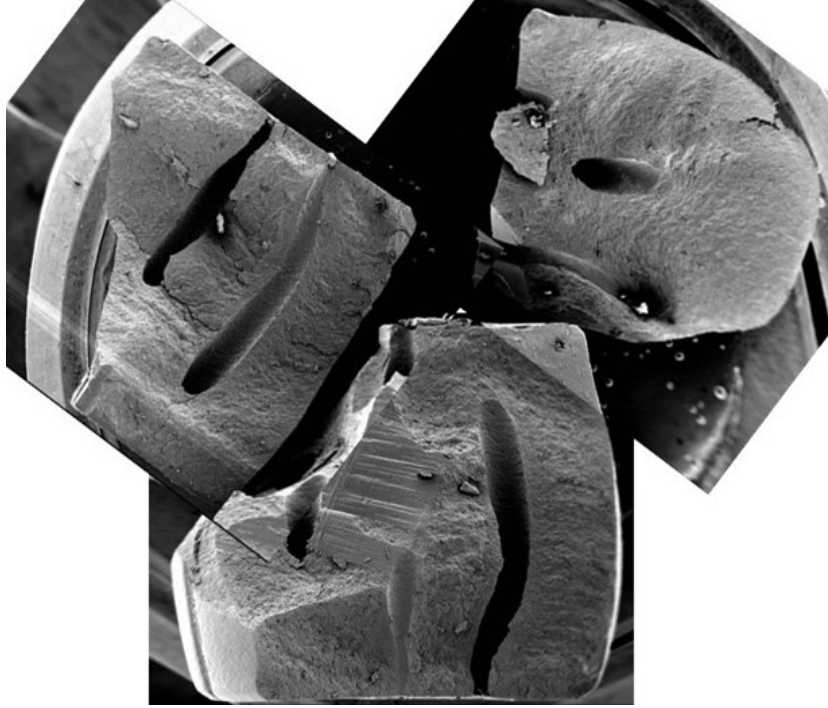
Fig. 55   SEM panorama of postcompression JA2 grain sample (uniaxially compressed at a rate of ~100 s^{-1}, –30 °C, and strain equal to 35%), 10× magnification
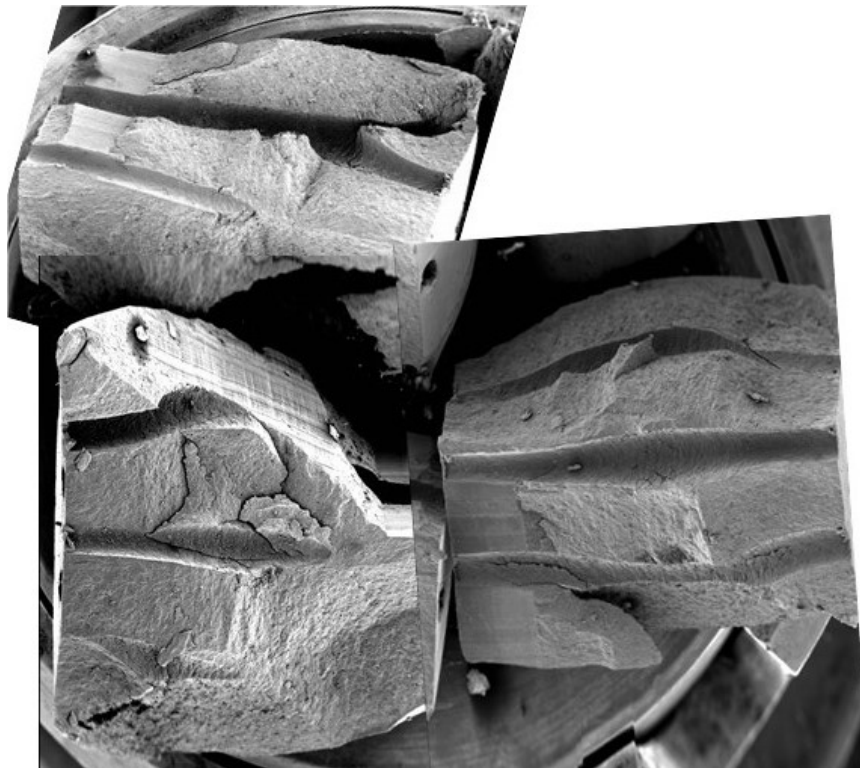
Fig. 56   SEM panorama of postcompression JA2 grain sample (uniaxially compressed at a rate of ~100 s^{-1}, –40 °C, and strain equal to 35%), 10× magnification
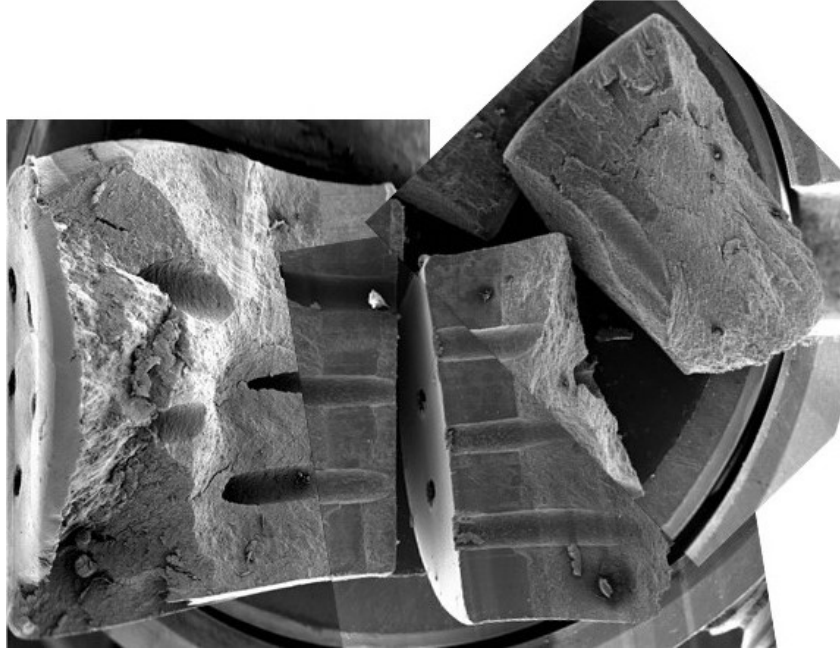
Fig. 57   SEM panorama of postcompression JA2 grain sample (uniaxially compressed at a rate of ~100 s⁻¹, –50 °C, and strain equal to 35%), 10× magnification
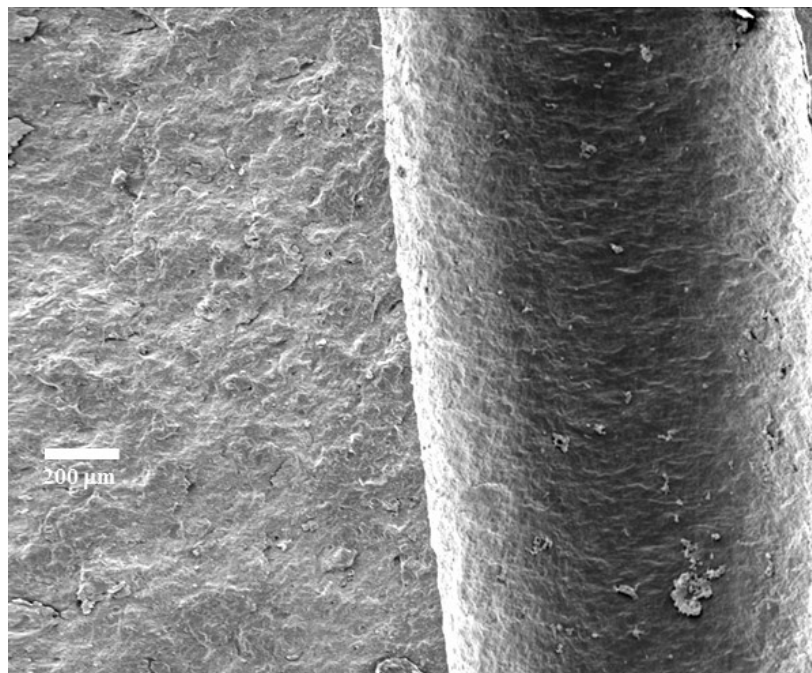
Fig. 58   SEM of postcompression JA2 grain sample (uniaxially compressed at a rate of ~100 s⁻¹, 60 °C, and strain equal to 35%), 50× magnification
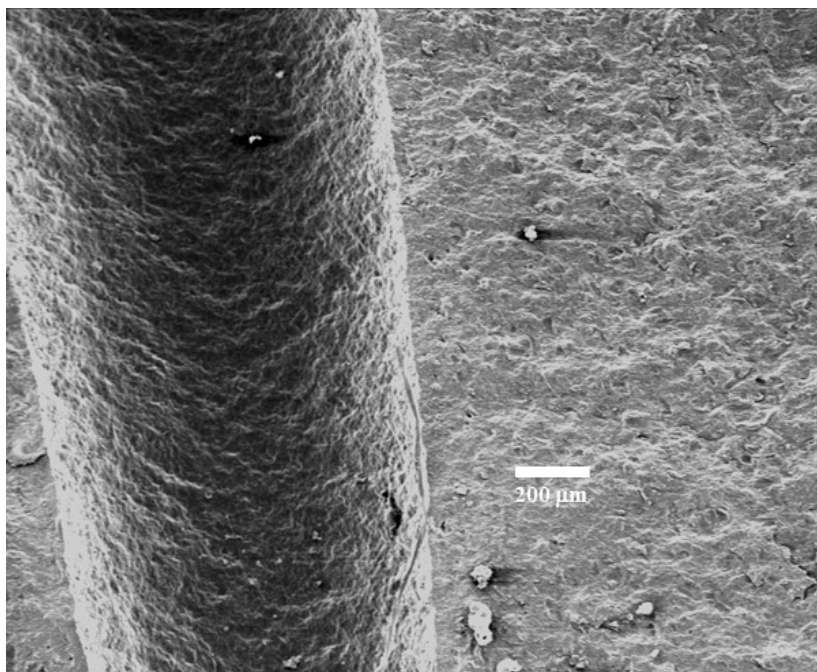
Fig. 59   SEM of postcompression JA2 grain sample (uniaxially compressed at a rate of ~100 s⁻¹, 40 °C, and strain equal to 35%), 50× magnification
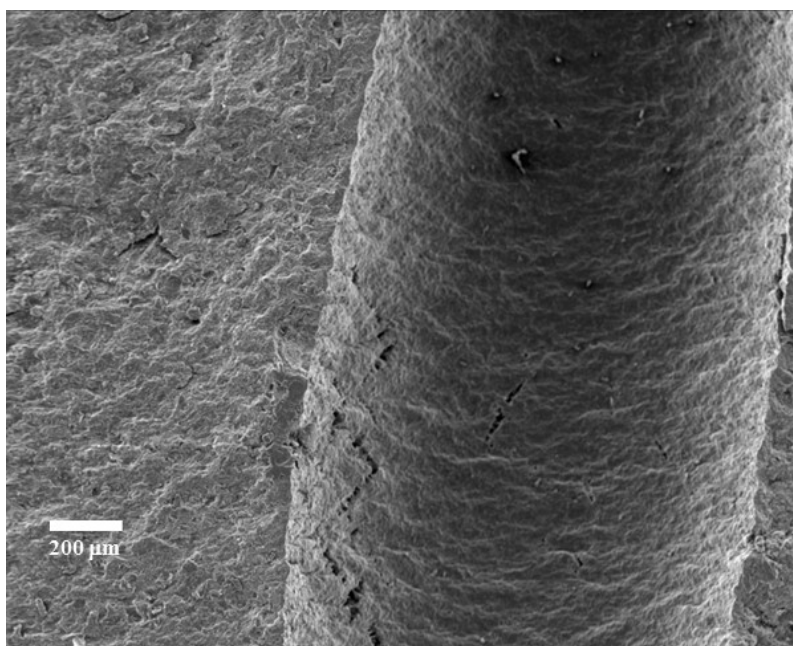
Fig. 60   SEM of postcompression JA2 grain sample (uniaxially compressed at a rate of ~100 s⁻¹, 20 °C, and strain equal to 35%), 50× magnification
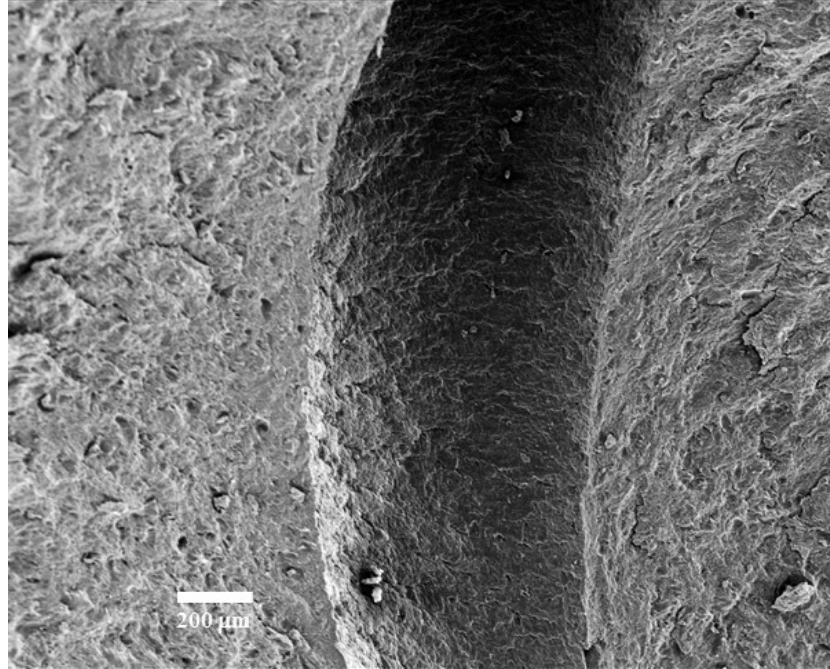
Fig. 61   SEM of postcompression JA2 grain sample (uniaxially compressed at a rate of ~100 s^{-1}, 0 °C, and strain equal to 35%), 50× magnification
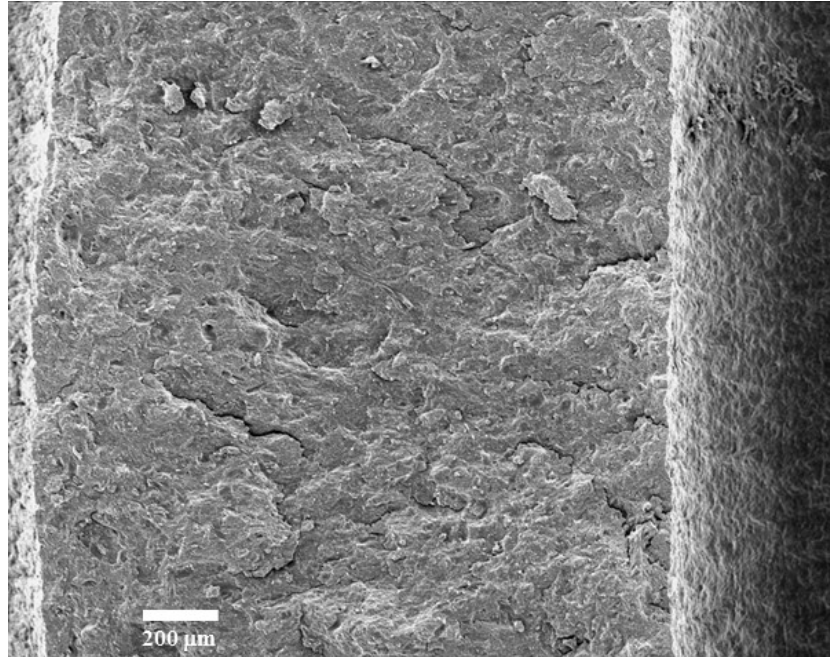
Fig. 62   SEM of postcompression JA2 grain sample (uniaxially compressed at a rate of ~100 s^{-1}, –10 °C, and strain equal to 35%), 50× magnification
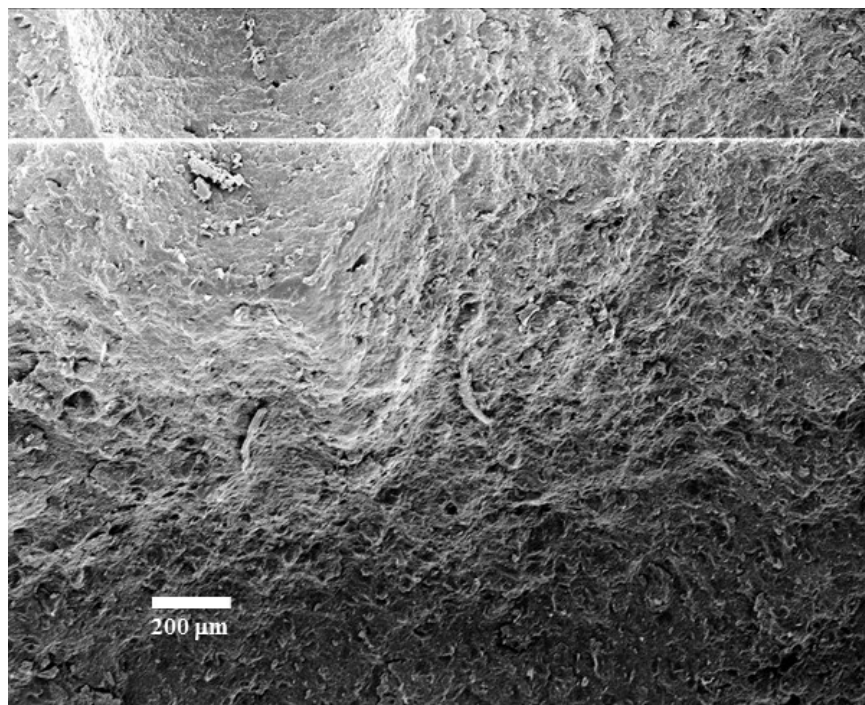
Fig. 63 SEM of postcompression JA2 grain sample (uniaxially compressed at a rate of ~100 s⁻¹, –20 °C, and strain equal to 35%), 50× magnification
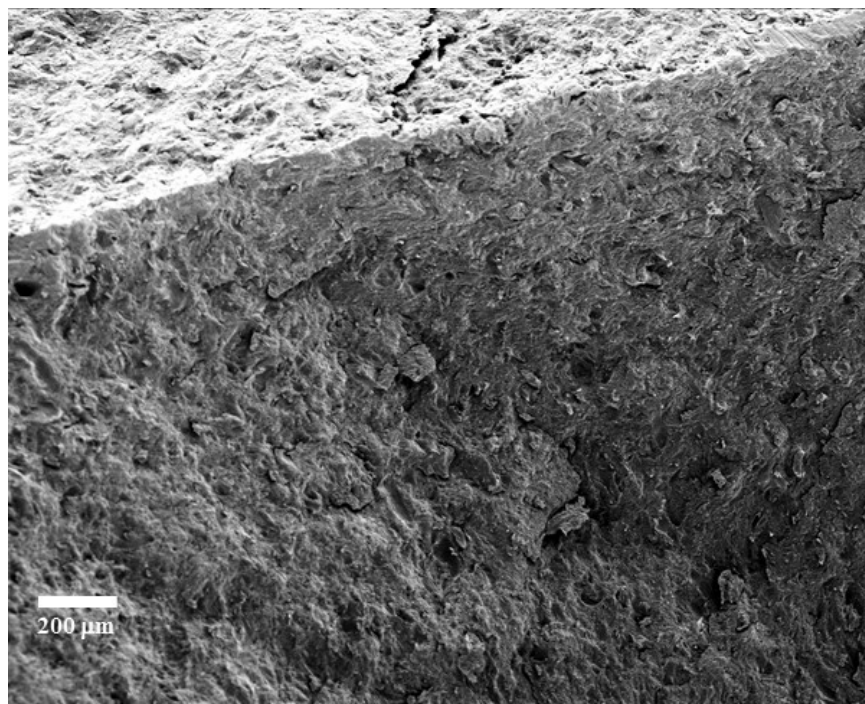
Fig. 64 SEM of postcompression JA2 grain sample (uniaxially compressed at a rate of ~100 s⁻¹, –30 °C, and strain equal to 35%), 50× magnification
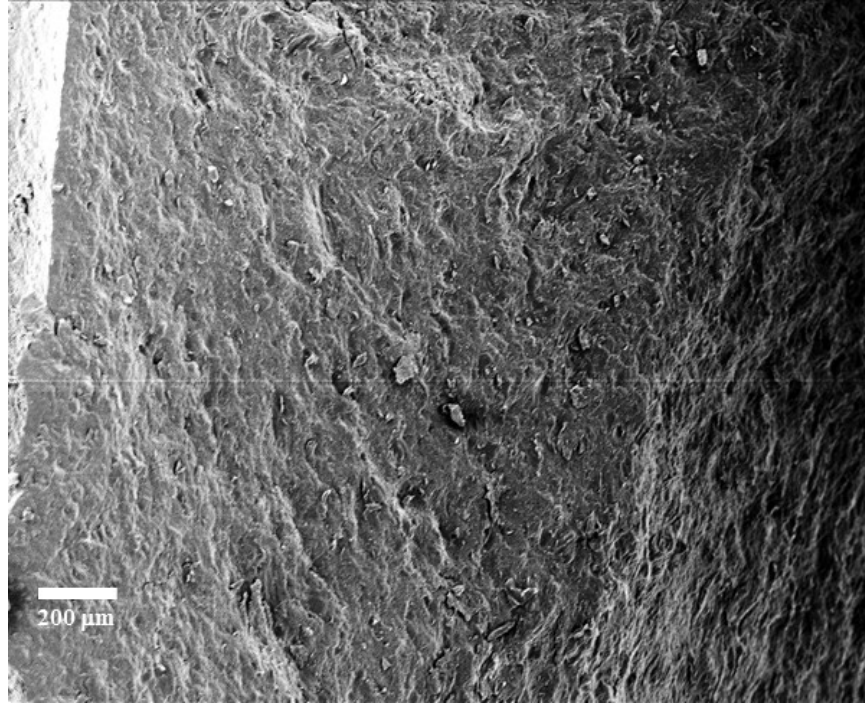
Fig. 65 **SEM panorama of postcompression JA2 grain sample (uniaxially compressed at a rate of ~100 s⁻¹, –40 °C, and strain equal to 35%), 50× magnification**
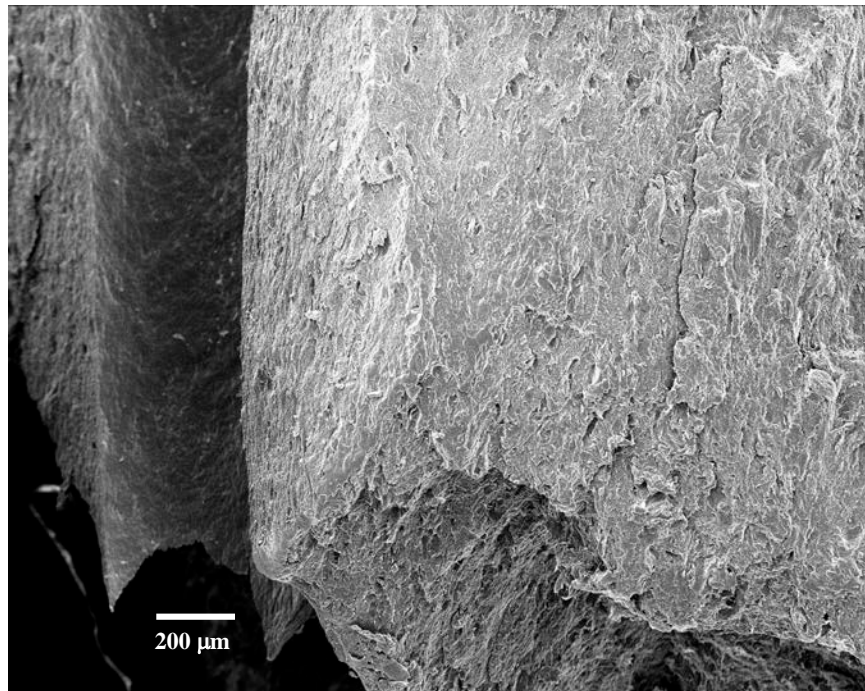
Fig. 66 **SEM panorama of postcompression JA2 grain sample (uniaxially compressed at a rate of ~100 s⁻¹, –50 °C, and strain equal to 35%), 50× magnification**

4. Conclusions

JA2, a viscoelastic propellant was examined for its mechanical properties under uniaxial compression at a ballistically relevant strain rate of approximately $100\ \text{s}^{-1}$ at each decade in temperature over the temperature range of 80 to –50 °C. At the hottest temperatures examined, the JA2 was initially in a rubbery or low viscosity state. An elastic region was not discernable at this scale in its stress-strain curve. It then work hardened to over 40% strain before structural failure began to occur. At temperatures near 60 °C and below, JA2 exhibited elastic behavior before yielding, followed by work hardening until failure at high strain.

SEM was used to determine the morphological state of the propellant after failure at high strain. This examination showed changes in the amount and modes of failure as the temperature decreased. Because this examination only showed the effects of full damage, the samples were repeated at an ultimate strain of approximately 35% (at or below the failure strain for the entire temperature range as shown in Figs. 6–19). At this strain, the stress-reducing modes were still in a formative state and could be examined. At temperatures above approximately 20 °C, plastic flow in the orthogonal direction to the compression was noted with microvoid formation more frequent as the temperature decreased. Below this temperature, microvoid formation and crack-tip propagation between voids seemed to dominate. However, by –20 °C it appeared that microvoid formation with fracture void to void dominated.

Interior ballistics modeling of the use of JA2 grains in a propelling charge will continue to evolve and improve. One improvement is to include grain fracture. If grain fracture is to be modelled accurately, the fracture trends as a function of temperature, strain, and strain rate will need to be known. The data in this report will need to be converted into constitutive relations for inclusion into the computer model. This conversion is beyond the scope of this report.

JA2 is also used as a reference for material properties in propellant development. Its resiliency over much of the service temperature range has been used as a standard to gage new propellants with regards to mechanical properties. With new elastomeric binders and polymeric exterior grain coatings the strain range of the standard, JA2, needed to be extended. The service temperature range for some ammunition propelling charges has been extended so the temperature range of the standard also needed to be extended. This report has accomplished both of these requirements.

5. References

1. Piraino SM, Leadore M, Meyer M, Lieb R, Horst A, Pesce-Rodriguez R. Characterization of the mechanical response of novel propellants. Aberdeen Proving Ground (MD): Army Research Laboratory (US); 2010 Aug. Report No.: ARL-TR-5293.

2. Manning TG, Rozumov E, Park D. Advanced high energy co-layered energetic thermoplastic elastomer (ETPE). Picatinny Arsenal (NJ): Army Armament Research, Development and Engineering Center (US); 2014 Jan. Report No.: ARMET-TR-12025.

3. Manning TG, Thompson D, Ellis M, Lieb R, Leadore M, Colburn J, Homan BE, Worrell DA, Moran KB, Ritchie SJ. Environmentally friendly green propellant for the medium caliber training rounds. Presented at the 34th Propellant and Explosives Development and Characterization Joint Army Navy NASA Air Force Interagency Propulsion Subcommittee Meeting, 2007 Aug 13–17, Reno, NV.

4. Gazonas GA, Hopkins DA, Ford JA. Experimental determination of critical physical parameters affecting JA2 propellant grain response, phase I: screening design. High-rate MTS SHT mechanical response and morphology of PAP8410 gun propellant. Aberdeen Proving Ground (MD): Ballistic Research Laboratory; 1991 May. Report No.: BRL-TR-3237.

5. Gazonas GA, Ford JA. Uniaxial compression testing of JA2 and M30 gun propellants using a statistical design strategy. Experimental Mechanics 1992;32(2):154.

6. Leadore MG, Lieb RJ. High-rate MTS SHT mechanical response and morphology of PAP8410 gun propellant. Aberdeen Proving Ground (MD): Army Research Laboratory (US); 2006 Apr. Report No.: ARL-TR-3771.

7. Lieb RJ. Correlation of the failure modulus to fracture-generated surface area in uniaxially compressed M43 gun propellant. Aberdeen Proving Ground (MD): Army Research Laboratory (US); 1995 Oct. Report No.: ARL-TR-884.

8. Leadore MG. MTS servo-hydraulic tester (SHT) mechanical properties evaluation of M43 propellants. Aberdeen Proving Ground (MD): Army Research Laboratory (US); 1993 Mar. Report No.: ARL-TN-5.

9. Leadore MG, Gillich CJ. Material testing system (MTS) servo-hydraulic tester (SHT) mechanical response of energetic thermal plastic elastomer (ETPE) RDX based propellants. Aberdeen Proving Ground (MD): Army Research Laboratory (US); 1994 Apr. Report No.: ARL-TN-28.

10. Howard SL, Leadore MG, Newberry JE, Kaste PJ. High-rate mechanical properties of Navy insensitive low erosion (NILE) propellant at temperatures from –40 to 70 °C. Aberdeen Proving Ground (MD): Army Research Laboratory (US); 2005 Jul. Report No.: ARL-TR-3546.

11. Hoffman HJ. Uniaxial compressive gun propellant test. In: Solid propellant mechanical behavior manual. Columbia (MD): Chemical Propulsion Information Analysis Center, The Johns Hopkins University; 1987 Nov. CPIAC Publication 21; Section 4.6.4.1.

12. Mulliken AD. Low to high strain rate deformation of amorphous polymers: experiments and modeling [master's thesis]. [Cambridge (MA)]: Massachusetts Institute of Technology; 2004.

13. Roesler J, Harders H, Baeker M. Mechanical behaviour of engineering materials: metals, ceramics, polymers and composites. New York (NY): Springer; 2007. p. 72.

14. Kukureka SN, Hutchings IM. Yielding of engineering polymers at strain rates of up to 500 s^{-1}. Int J Mech Sci. 1984:11/12:617.

15. Bowden PB. The yield behaviour of glassy polymers. In: Haward RN, editor. Physics of glassy polymers. London (UK): Applied Science; 1973. p. 279.

16. Christensen RM. Observation on the definition of yield stress. Acta Mech. 2008;196:239–244.

17. Howard SL. Constitutive relations of selected propellants at temperatures from –50 °C to 80 °C. Aberdeen Proving Ground (MD): Army Research Laboratory (US); 2016. Forthcoming.

18. Howard SL, Leadore MG. Heat distortion measurements of standard and research gun propellants. Aberdeen Proving Ground (MD): Army Research Laboratory (US); 2015 Mar. Report No.: ARL-TR-7222.

19. Saenz EE, Carlsson LA, Karlsson AM. In situ analysis of crack propagation in polymer foams. J Mat Science. 2011;46(16):5487–5494.

20. Chiang F-P, Chang S, Ding Y. Crack tip strain field and its propagation characteristics in a polymer foam. In: Gdoutos EE, editor. Fracture of nano and engineering materials and structures: proceedings of the 16th European conference of fracture; 2006 July 3–7; Alexandroupolis, Greece. Vol. 10. Berlin (Germany): Springer; c2006. p. 89–90.

INTENTIONALLY LEFT BLANK.